colonocytes and to have a low retrieval rate. Accordingly, the sensitivity of this mRNA-based method also appears to be insensitive.

In any method for colorectal cancer detection using feces, an effective method which allows the simple isolation of the colonocytes from not only the surface but also the central portion of the feces while maintaining the initial morphology is needed. Recently, we successfully developed a new, very effective method that is based on the filtration of the homogenates of feces and magnetic cell sorting (MACS) with an epithelial cell-specific antibody, which we here abbreviated to FMCI (filtration and MACS-based colonocyte isolation) (23). It has been shown that this method can provide a high quality of colonocyte DNA or RNA for molecular biological analysis and also provide the colonocyte with its original morphology for cytology. Considering the advantage in the use of FMCI, we here report expression profiling of colonocytes for fecal RNA-based detection of curable colorectal cancer and a sensitive focused microarray assay that uses multiple marker genes for detecting minimal cancer cells in the feces of patients with colorectal cancer.

Materials and methods

Clinical materials. This study protocol was reviewed and approved by the Institutional Review Board of the National Cancer Center, Tokyo. Written informed consent was obtained from all the patients and healthy volunteers. Before surgical resection, stool samples were obtained from 23 patients with colorectal cancer (Dukes stages A-C), for which curable resection is possible, and from 15 healthy volunteers a few weeks after they had undergone a total colonoscopy. Naturally evacuated feces from subjects who had not taken laxatives were used as stool samples. Each patient was instructed to evacuate into a polystyrene disposable tray (AS one, Osaka, Japan) measuring 5x10 cm in size. Preparation of the stool samples for examination was conducted within 1-6 h after the evacuation. Tissue samples were obtained from the surgically resected specimens of colorectal cancer patients, and were snap frozen in liquid nitrogen and stored at -80°C until use. RNA of the tissues was extracted by using an Isogen kit (Nippon Gene, Toyama, Japan). The peripheral blood samples of 58 healthy volunteers and their RNA were prepared as in our previous report (24).

Isolation of exfoliated cells from feces. The procedure is detailed in our previous report (23). In brief, approximately 5-10 g of feces was used to isolate exfoliated cells. Feces were collected in Stomacher Lab Blender bags (Seward, Thetford, UK). The stool samples were homogenized with a buffer (200 ml) consisting of Hank's solution, 25 mM Hepes (pH 7.35), and 10% fetal bovine serum at 200 rpm for 1 min using a Stomacher (Seward). The homogenates were then filtered through a nylon filter (pore size, 512 μm), followed by division into 5 portions (40 ml each). Subsequently, 40 μl of magnetic beads coated with a mouse IgG1 monoclonal antibody (mAb Ber-EP4) specific for the glycopolypeptide membrane antigen Ep-CAM, which is expressed on most normal and neoplastic human epithelial cells (Dynal, Oslo, Norway), was added to each portion, and the mixtures were incubated for 30 min under gentle rolling in a mixer at room temperature. After 15-min shaking, the colonocytes were recovered from 5 tubes. The colonocytes from a single tube were stored at -80°C for RNA extraction. The colonocyte RNA was extracted by using an Isogen kit (Nippon Gene, Toyama, Japan).

Microarray analysis. We used human U133A Gene Chip (Affymetrix, Santa Clara, CA) for genome-wide expression profiling of mRNAs corresponding to 14,564 genes, 18,445 transcripts including splicing variants, and 22,215 probe sets. The procedures were conducted according to the supplier's protocols. Briefly, 10 μg of fragmented cRNA was hybridized to the microarrays in 200 μl of a hybridization cocktail at 45°C for 16 h in a rotisserie oven set at 60 rpm. The arrays were then washed with a nonstringent wash buffer (6X SSPE) at 25°C, followed by a stringent wash buffer [100 mM MES (pH 6.7), 0.1 M NaCl, and 0.01% Tween-20] at 50°C, stained with streptavidin phycoerythrin (Invitrogen, Carlsbad, CA), washed again with 6X SSPE, stained with biotinylated anti-streptavidin IgG, followed by a second staining with streptavidin phycoerythrin and a third wash with 6X SSPE. The arrays were scanned using a GeneArray scanner (Affymetrix) at 3-μm resolution, and the expression value (average difference: AD) of each gene was calculated using GeneChip Analysis Suite version 5.0 software (Affymetrix). The mean of AD values in each experiment was 1000 to reliably compare variable multiple arrays.

Reverse transcription-polymerase chain reaction (RT-PCR). RT-PCR on colonocyte RNA was carried out using primer sets designed for detecting the 3' side of cDNA of each gene. Primers were 5'-ACCAGTGTGAGGACTCACCC-3' and 5'-TGCTCTTTAAAGCCTTAGGCC-3' for PAP; 5'-AGCAATTACAACGGAGTCAA-3' and 5'-TCCAAAGACTGGGGTAGGT-3' for REGIA; 5'-TCTCTCCTGTGAAACCTGGG-3' and 5'-AAGGGGTGTTGCTTTTATTGC-3' for DPEP1; 5'-ATTAGCAGTTTAGAATGGAGG-3' and 5'-CTGTATCCAATTCTGTACTGC-3' for SEPP1; 5'-TGGGCTGCCAACATGCCATC-3' and 5'-TGTAGTAGCCCGATCGCACC-3' for RPL27A; 5'-GGCAAGCGAGATGAAGATAAGG-3' and 5'-AGGTCCCATACGTATGACAG-3' for ATP1B1; 5'-AGACTATCCACCTTTGGGTCG-3' and 5'-GATGCATTGTTATCATTAACCAGTC-3' for EEF1A; 5'-TTGAGCGCACCTAACCACTGGT-3' and 5'-GAGAGGAAACATGGTCACACCCA-3' for SFN, and 5'-ACATTCAGACTGAGCGTGCCTA-3' and 5'-GATCTGGACGTCCCTGAAGCA-3' for RPS11. PCR was performed under conditions of 30-35 cycles of 3 steps of temperature, 95°C for 1 min, 55°C for 1 min, and 72°C for 1 min, using the AccuPrime TaqDNA polymerase system (Invitrogen).

Marker gene detection using focused microarray. A focused microarray was constructed by fixing 50-60 mer of oligonucleotide probes on a slide glass using our previously developed Bubble Jet Technology (25). The microarray contained a single spot for each sequence of 9 marker genes (PAP, REG1A, DPEP1, SEPP1, RPL27A, ATP1B1, EEF1A1, SFN, and RPS11) and a control artificial DNA sequence. Each probe sequence used for the microarray is listed in Table I.

Table I. Sequences of primers and probes for focused microarray analysis.

Gene	Forward primers Reverse primers	Probes
PAP	GAGAAGCACAGCATTTCTGAG TGCTCTTTAAAGCCTTAGGCC	TTCCCCCAACCTGACCACCTCATTCTTATCTTTCTTCTGT TTCTTCCTCCCCGCTGTCAT
REG1A	AATCCTGGCTACTGTGTGAG TCCAAAGACTGGGGTAGGT	GACCATCTCTCCAACTCAACTCAACCTGGACACTCTCTT CTCTGCTGAGTTTGCCTTGTT
DPEP1	ACCCATTACGGCTACTCCTC AAGGGGTGTTGCTTTTATTGC	CAGATGCCAGGAGCCCTGCTGCCCACATGCAAGGACCA GCATCTCCTGAGAG
SEPP1	AATTAGCAGTTTAGAATGGAGG CTGTATCCAATTCTGTACTGC	CCATAGTCAATGATGGTTTAATAGGTAAACCAAACCCTA TAAACCTGACCTCCTTTATGG
RPL27A	TGGGCTGCCAACATGCCATC TGTAGTAGCCCGATCGCACC	CCAACTGTCAACCTTGACAAATTGTGGACTTTGGTCAGT GAACAGACACGGGTGAATGCT
ATP1B1	GGCAAGCGAGATGAAGATAAGG AGGTCCCATACGTATGACAG	GAGTGTAAGGCGTACGGTGAGAACATTGGGTACAGTGA GAAAGACCGTTTTCAGGGACGT
EEF1A1	AGACTATCCACCTTTGGGTCG GATGCATTGTTATCATTAACCAGTC	CCACCCCACTCTTAATCAGTGGTGGAAGAACGGTCTCAG AACTGTTTGTTTCAATTGGCC
SFN	TTGAGCGCACCTAACCACTGGT GAGAGGAAACATGGTCACACCCA	CTCTGATCGTAGGAATTGAGGAGTGTCCCGCCTTGTGGC TGAGAACTGGACAGTGG
RPS11	ACATTCAGACTGAGCGTGCCTA GATCTGGACGTCCCTGAAGCA	TCATCCGCCGAGACTATCTGCACTACATCCGCAAGTACA ACCGCTTCGAGAAGCG

Focused microarray analysis consists of 3 steps: i) Cy3-dUTP labeling by multiplex-RT-PCR; ii) hybridization Cy3-labeled cDNA to microarray, and iii) fluorescence scanning (Fig. 3). Using 0.5 to 1 μg of total RNA prepared from colonocytes, reverse transcription was performed with Superscript II (Invitrogen) with T7-oligo dT 24 primer in a total volume of 20 μl according to the manufacturer's protocol. To obtain 5-10 μg of cRNA, T7 transcription was performed. Using 5-10 μg of the cRNA, reverse transcription was performed with Superscript II with random hexamer in a total volume of 20 μl. Multiplex-RT-PCR was performed in two tubes at different PCR cycles: 35 cycles for PAP, REG1A and DPEP1, and 25 cycles for SEPP1, RPL27A, ATP1B1, EEF1A1, SFN, and RPS11. PCR primer sequences are also listed in supplementary Table II. Twenty-five μl of the PCR solution in each tube consisted of 1 μl of template cDNA, primers (6.25 pmol each), 50 μM Cy3-dUTP, 2.5 μl of AccuPrime 10X buffer1 (2 mM dNTP, 15 mM $MgCl_2$) and 1.0 μl of AccuPrime Taq polymerase (Invitrogen). A thermal cycler was set with initial heating at 95°C for 5 min followed by an amplification cycle heated at 95°C for 30 sec, 58°C for 30 sec and 72°C for 40 sec, followed by heating at 72°C for 10 min. The two PCR solutions were mixed and purified with a QIAquick PCR purification kit (Qiagen, Tokyo, Japan). The entire Cy3-labeled cDNA solution (50 μl) was mixed in 120 μl of a hybridization cocktail (6X SSPE containing 900 mM NaCl, 60 mM NaH_2PO_4, and H_2O, and 6 mM EDTA, pH 7.4/ 10% formamide/0.05% SDS) including 0.1 nM Cy3-labeled oligonucleotide which hybridizes the control artificial DNA sequence. By using a hybridization apparatus, HybStation (Genomic Solutions, Ann Arbor, MI), an array was pre-heated to 65°C for 3 min, filled with the hybridization cocktail, and incubated at 92°C for 2 min and then at 55°C for 4 h. Subsequently, the array was washed with 2X SSC, 0.1% SDS at 25°C and then with 2X SSC at 20°C, and rinsed with 0.1X SSC in accordance with a conventional manual, and finally dried by a spin drier. The array was scanned by an apparatus for DNA microarrays, Genepix 4000B (Axon Instruments, Union City, CA) and the fluorescence intensity from each probe spot was obtained after subtracting the background level. This focused microarray assay belongs in a negative or positive assay. However, it is required for determining the cutoff values. In this study, the maximum value of each gene plus 2- or 3-times standard deviation in 7 healthy volunteers was used as the cutoff-value.

Results

Marker gene selection through genome-wide expression profiles of cancer tissues, non-cancerous tissues, and the peripheral blood. In the feces of colorectal cancer patients, living cells other than bacteria include a small amount of cancer cells and normal colorectal mucus cells, lymphocytes, red blood cells and anal squamous cells. It is noted that the content of lymphocytes and red blood cells is increased in the feces of people with hemorrhoids. Therefore, genes that are expressed in almost all cases of early and advanced colorectal cancer and that are not expressed in normal colorectal mucosas,

Table II. Eighty-five genes expressed in the cancer patient-derived colonocytes but not in the healthy volunteer-derived colonocytes.

No.	Gene symbol	Gene title	Entrez gene ID	No expression in the PB
1	JUND	jun D proto-oncogene	3727	
2	TPT1	tumor protein, translationally-controlled 1	7178	*
3	RPL41	ribosomal protein L41	6171	*
4	RPS11	ribosomal protein S11	6205	*
5	RPS29	ribosomal protein S29	6235	*
6	RPL38	ribosomal protein L38	6169	*
7	SEPP1	selenoprotein P, plasma, 1	6414	*
8	RPL23	ribosomal protein L23	9349	*
9	B2M	ß-2-microglobulin	567	*
10	CFL1	cofilin 1 (non-muscle)	1072	*
11	RPL31	ribosomal protein L31	6160	*
12	RPS3A	ribosomal protein S3A	6189	
13	TMSB10	thymosin, ß 10	9168	*
14	RPL39	ribosomal protein L39	6170	*
15	HMGB1	high-mobility group box 1	3146	*
16	CEACAM6	carcinoembryonic antigen-related cell adhesion molecule 6 (non-specific cross reacting antigen)	4680	
17	ATP1B1	ATPase, Na^+/K^+ transporting, ß 1 polypeptide	481	*
18	RPS20	ribosomal protein S20	6224	*
19	ARF6	ADP-ribosylation factor 6	382	*
20	RPS21	ribosomal protein S21	6227	*
21	EIF5A	Eukaryotic translation initiation factor 5A	1984	*
22	RPL30	ribosomal protein L30	6156	*
23	EEF1A1	eukaryotic translation elongation factor 1 α 1	1915	*
24	RPL23A	ribosomal protein L23a	6147	*
25	LOC56902	putatative 28 kDa protein	56902	
26	RPL27	ribosomal protein L27	6155	*
27	SFN	stratifin	2810	*
28	CEACAM5	carcinoembryonic antigen-related cell adhesion molecule 5	1048	*
29	RPS24	ribosomal protein S24 /// ribosomal protein S24	6229	*
30	MARCKS	Myristoylated alanine-rich protein kinase C substrate	4082	*
31	PDE4C	phosphodiesterase 4C, cAMP-specific (phosphodiesterase E1 dunce homolog, *Drosophila*)	5143	
32	LOC651423	similar to mitogen-activated protein kinase kinase 3 isoform A	651423	
33	RPS10	ribosomal protein S10	6204	
34	CEP27	centrosomal protein 27 kDa	55142	
35	IL1RN	interleukin 1 receptor antagonist	3557	*
36	SLC35E1	solute carrier family 35, member E1	79939	
37	RPS27	ribosomal protein S27 (metallopanstimulin 1)	6232	*
38	RPS19	ribosomal protein S19	6223	*
39	RPS16	ribosomal protein S16	6217	*
40	MORF4L2	mortality factor 4 like 2	9643	*
41	RPL22	ribosomal protein L22	6146	*
42	RPS2	ribosomal protein S2	6187	*
43	RPLP2	ribosomal protein, large, P2	6181	*
44	RPL7A	ribosomal protein L7a	6130	
45	RPL7	ribosomal protein L7	6129	
46	RPS18	ribosomal protein S18	6222	*
47	HNRPH1	Heterogeneous nuclear ribonucleoprotein H1 (H)	3187	*
48	ZNF160	zinc finger protein 160	90338	

Table II. Continued.

No.	Gene symbol	Gene title	Entrez gene ID	No expression in the PB
49	RPS25	ribosomal protein S25	6230	*
50	PGF	Placental growth factor, vascular endothelial growth factor-related protein	5228	
51	SPG21	spastic paraplegia 21 (autosomal recessive, Mast syndrome)	51324	
52	RPL9	ribosomal protein L9	6133	*
53	PLEKHA5	Pleckstrin homology domain containing, family A member 5	54477	
54	PRR11	proline rich 11	55771	
55	CTNNB1	catenin (cadherin-associated protein), ß 1, 88 kDa	1499	*
56	NFKBIA	nuclear factor of κ light polypeptide gene enhancer in B-cells inhibitor, α	4792	*
57	GTSE1	G-2 and S-phase expressed 1	51512	
58	ATP8B1	ATPase, Class I, type 8B, member 1	5205	
59	TMED2	transmembrane emp24 domain trafficking protein 2	10959	*
60	RPS4X	ribosomal protein S4, X-linked	6191	
61	MUC3B	mucin 3B, cell surface associated	57876	
62	TTLL12	tubulin tyrosine ligase-like family, member 12	23170	
63	FTL	ferritin, light polypeptide	2512	*
64	TSPAN13	Tetraspanin 13	27075	*
65	PTP4A2	protein tyrosine phosphatase type IVA, member 2	8073	*
66	EGLN3	egl nine homolog 3 (C. elegans)	112399	*
67	ROCK2	Rho-associated, coiled-coil containing protein kinase 2	9475	
68	NDRG1	N-myc downstream regulated gene 1	10397	*
69	GTPBP1	GTP binding protein 1	9567	*
70	CAPZA1	capping protein (actin filament) muscle Z-line, α 1	829	*
71	RPL13	ribosomal protein L13	6137	*
72	CIDEC	cell death-inducing DFFA-like effector c	63924	*
73	SIRT3	sirtuin (silent mating type information regulation 2 homolog) 3 (S. cerevisiae)	23410	
74	LAPTM4A	lysosomal-associated protein transmembrane 4 α	9741	*
75	NOS1	nitric oxide synthase 1 (neuronal)	4842	*
76	COQ10B	coenzyme Q10 homolog B (S. cerevisiae)	80219	*
77	SAT	spermidine/spermine N1-acetyltransferase	6303	*
78	C1orf107	chromosome 1 open reading frame 107	27042	
79	TXN	thioredoxin	7295	*
80	SLC7A1	solute carrier family 7 (cationic amino acid transporter, y^+ system), member 1	6541	
81	SLC1A7	solute carrier family 1 (glutamate transporter), member 7	6512	
82	VIL2	villin 2 (ezrin)	7430	*
83	NTRK2	neurotrophic tyrosine kinase, receptor, type 2	4915	
84	GSTA1	Glutathione S-transferase A1	2938	
85	PTP4A3	protein tyrosine phosphatase type IVA, member 3	11156	

(*) Genes that were expressed in the cancer patient-derived colonocytes but not in either the healthy volunteer-derived colonocytes or the peripheral blood (PB) mixture.

peripheral blood, and squamous cells are potentially good markers for the screening of colorectal cancer from the feces. To identify effective genes for fecal RNA-based screening, we first compared 10 gene expression profiles of 6 early colorectal cancer tissues (2 Dukes stage A and 4 Dukes stage B cases), 3 advanced cancer RNA mixtures (6, 6, and 7 Dukes stage C or D cases), and a normal colorectal mucosa RNA mixture (6 cases). Of 14,564 genes, 2,926 were identified as genes which were not detected in the normal mucosa but detected in at least one of the above 9 cancer samples. Among these 2,926 cancer-specific genes, 205 genes, which were expressed in all of the 3 advanced cancer mixtures, were identified; however, only 3 genes were found to be expressed in all of the 6 early cancers. The cause of these results may

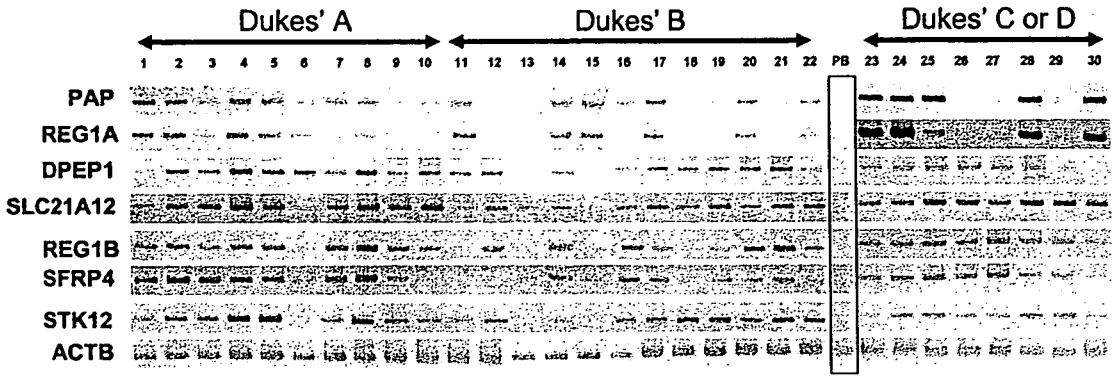

Figure 1. Results of RT-PCR of 7 genes (PAP, REG1A, DPEEP1, SLC21A12, REG1B, SFRP4, and STK12) selected by microarray analysis on 30 colorectal cancer tissues and on a peripheral blood mixture (PB). By microarray analyses, we first identified 15 genes which were expressed not in the normal colorectal mucosa mixture or in a peripheral blood mixture but in more than 4 of 6 early cancers (Dukes stage A or B) and in all of 3 advanced cancer mixtures (Dukes stage C or D). Next, we examined the frequency of the expression of these 15 genes in 30 colorectal cancer tissues (10 Dukes stage A, 12 Dukes stage B, and 8 Dukes stage C or D cancers), and selected, by RT-PCR, 7 genes (PAP, REG1A, DPEP1, SLC21A12, REG1B, SFRP4, and STK12) as the frequently expressed genes at any stage of colorectal cancer.

be that the expression profile of early cancer varies from case to case. Of 14,564 genes, we were able to select 65 genes which were expressed not in the normal colorectal mucosa mixture but in more than 4 of the 6 early cancers and in all of the 3 advanced cancer mixtures.

Considering bleeding by nonmalignant diseases such as hemorrhoids, which often give false positives in fecal colorectal cancer screening, we selected 15 genes from the 65 genes, because the expression of all the other 50 genes was detectable in a peripheral blood mixture of 58 healthy volunteers when a highly sensitive nested RT-PCR analysis with outer and inner primer sets was performed (data not shown). Next, we examined the frequency of the expression of these 15 genes in 30 colorectal cancer tissues (10 Dukes stage A, 12 Dukes stage B, and 8 Dukes stage C or D cancers), and selected, by RT-PCR, 7 genes (PAP, REG1A, DPEP1, SLC21A12, REG1B, SFRP4, and STK12) as the frequently expressed genes at any stage of colorectal cancer (Fig. 1). By RT-PCR, we lastly checked the expression of these 7 genes in RNA samples of the colonocytes of 15 healthy volunteers, which were isolated from the feces by FMCI (23). No mRNA expression of 3 genes (PAP, REG1A, and DPEP1) was detected in the colonocyte samples of all the 15 healthy volunteers; however, the other 4 genes (SLC21A12, REG1B, SFRP4, and STK12) were found to be expressed in some samples (data not shown). This fact may be due to the contamination of anal squamous cells, which were dissociated from the anus and survived in the feces, because our gene selection process can minimize the effect on the contamination of lymphocytes, red blood cells and dissociated normal colorectal epithelium. Under the above criteria, only 3 genes were selected as the final candidates for the fecal RNA-based early detection of colorectal cancer.

Marker gene selection by comparison of expression profiles between healthy volunteer- and cancer patient-derived colonocytes from the feces. Next, we obtained and compared 5 gene expression profiles of 4 colonocyte RNA samples (CF15, CF17, CF18, and CF25), which were isolated from the feces of 4 colorectal cancer patients by FMCI, and a colonocyte RNA mixture (HVF) of 7 healthy volunteers. Of 14,564 genes, the number of detectable genes in 5 colonocyte samples, CF15, CF17, CF18, CF25, and HVF is 768, 603, 772, 459, and 326, respectively. The number of detectable genes in the colonocyte is approximately 6.5% of that (11,343) in the colorectal cancer tissue. The major reason seems to be that most colonocytes are not in the cell division cycle but are resting, because the detectable gene number (1,535) in the peripheral blood composing such resting cells was also small. Unexpectedly, 716 (93%), 553 (92%), 712 (92%), and 424 (92%) of the above detectable genes (768, 603, 772, and 459) in the the colonocytes of the cancer patients were not expressed in those of the healthy volunteers. The huge difference of the colonocyte expression profiles between the colorectal cancer patients and the healthy volunteers might lead to success in gene selection for fecal RNA-based early detection of colorectal cancer. Eighty-five genes, whose expression was found in 3 or 4 of the 4 colorectal cancer patient samples (CF15, CF17, CF18, and CF25) but not in the HVF, were identified (Table II). Of these 85 genes, 29 (34%) were found to encode ribosomal proteins (RPLs or RPSs). In the course of a series of studies, it is predicted that normal mucous cells will die and be exfoliated during turnover and that the colorectal cancer cells will survive for a long time in the isolation processes as well as in the feces (22,23). Therefore, protein synthesis in the cells would be maintained actively for cancer cell survival under these conditions. The FMCI can minimize the contamination of both lymphocytes and red blood cells because the FMCI contains the enrichment process of epithelial cells such as colorectal cancer cells, the contaminated anal squamous cells, and a few living cells dissociated from the normal colorectal mucosa by MACS (23). Therefore, expression status in the peripheral blood is not needed for the gene selection process for fecal RNA-based screening; all of the 85 genes are expected to be good markers if the colonocytes are isolated by FMCI.

RT-PCR and focused microarray analyses of 9 selected genes in 30 colonocyte RNA samples. Next, we performed RT-PCR of the first 3 identified genes (PAP, REG1A, and DPEP1) in the colonocyte RNA samples which were prepared from 23 curable colorectal cancer patients (Dukes stages A-C) and 7 healthy volunteers. The 23 colorectal cancer patients were 8

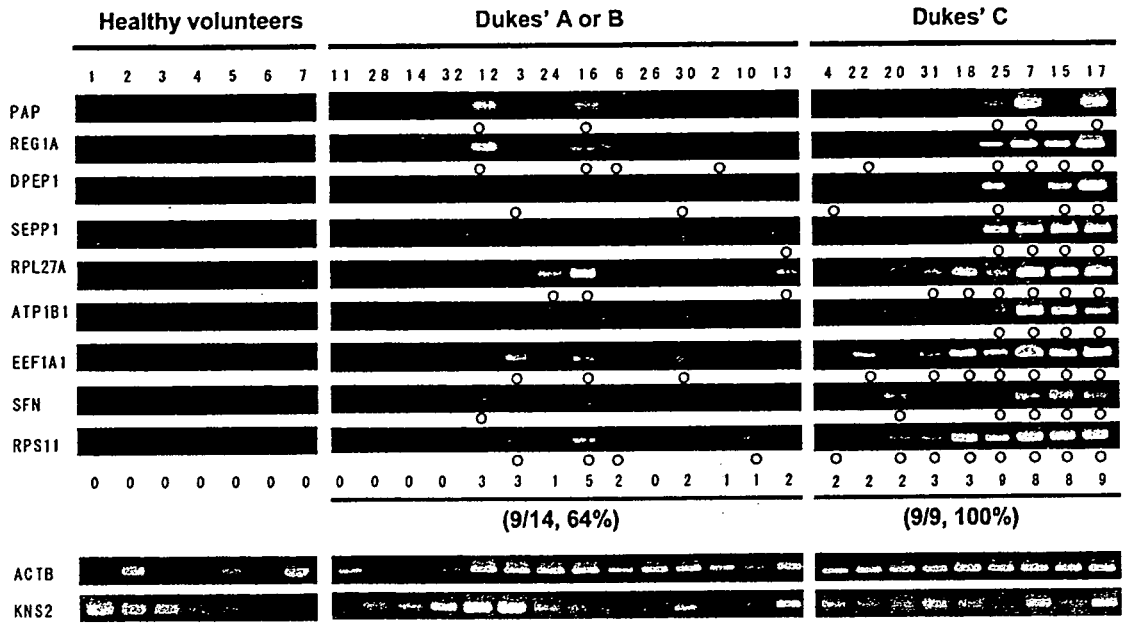

Figure 2. Results of RT-PCR of 9 genes (PAP, REG1A, DPEEP1, SEPP1, RPL27A, ATP1B1, EEF1A1, SFN, and RPS11) in the colonocyte RNA samples from 23 curable colorectal cancer patients and 7 healthy volunteers. We performed RT-PCR of the first 3 identified genes (PAP, REG1A, and DPEP1) in the colonocyte RNA samples which were prepared from 23 curable colorectal cancer patients (8 Dukes stage A, 6 Dukes stage B, and 9 Dukes stage C) and 7 healthy volunteers. Next, to test the power of the 85 genes, which were identified by colonocyte gene expression profiling, we randomly selected 6 (SEPP1, RPL27A, ATP1B1, EEF1A1, SFN, and RPS11), and performed RT-PCR on the same samples. In total, RT-PCR of those 9 genes detected 18 (78%) of the 23 cancer patients, and 9 (64%) of the 14 early cancers (Dukes stage A or B) were detected; however, the expression of all of the 7 genes was hardly detected in the 7 healthy volunteers (upper panel). The expression level of housekeeping genes such as ACTB (ß-actin) was highly varied from sample to sample (lower panel). KNS2 encoding kinesin 2 was selected, by microarray analyses, as a gene expressed constantly in any colonocyte RNA sample; however, the expression level was also varied. Open circles indicate positive RT-PCR product, and numbers indicate the number of the positive genes in each sample.

with Dukes stage A, 6 with Dukes stage B, and 9 with Dukes stage C cancers; 5 were right-sided and 18 were left-sided cancers. Twelve (52%) of the 23 cancers were positive by RT-PCR in at least one of the 3 genes whereas no positive gene was found in any of the healthy volunteers (Fig. 2). To test the power of the 85 genes, which were identified by colonocyte gene expression profiling, we randomly selected 6 (SEPP1, RPL27A, ATP1B1, EEF1A1, SFN, and RPS11). RT-PCR of these 6 genes detected 16 (70%) of the 23 cancers as at least positive for 1 gene whereas no positive gene was found in any of the healthy volunteers (Fig. 2). No or a quite low signal of all the 9 genes was found in another RT-PCR experiment with 8 healthy volunteers (data not shown). In total, RT-PCR of those 9 genes detected 18 (78%) of the 23 cancer patients (Fig. 2). The 18 patients detected were 4 with Dukes stage A, 5 with Dukes stage B, and 9 with Dukes stage C cancers; 4 were right-sided and 14 were left-sided cancers. Therefore, 9 (64%) of the 14 early cancers (Dukes stage A or B), which have no lymph node metastasis, and show a good prognosis, were able to be detected. Importantly, 4/5 (80%) of the right-sided colorectal cancers were detected, which have been reported to be very difficult to detect by any feces-based molecular biological method, because most right-sided cancer-derived colonocytes are severely damaged from remaining for a long time in the feces.

For fecal RNA-based detection of early colorectal cancer, quantitative real-time RT-PCR is thought to hardly apply in the colonocyte because the expression level of housekeeping genes was highly varied from sample to sample (Fig. 2). The expressional variation could be explained by the difference of the physiological condition of colorectal cancer cells and anal squamous cells isolated from the feces by FMCI. All of the 9 genes were selected as cancer cell- or cancer patient-derived colonocyte-specific genes. Therefore, a negative or positive assay was thought to be sufficient for fecal RNA-based colorectal cancer detection. Accordingly, we developed a multiplex RT-PCR-based microarray assay for evaluating the above RT-PCR results and for providing an effective imaging tool for mass cancer screenings (Fig. 3). The Cy3-labeled cDNAs prepared by multiplex RT-PCR in a single tube were hybridized with 9 gene sequences on a focused microarray, which was manufactured by our previously developed Bubble Jet Technology with a small modification (25). Hybridization signals and the number of positive genes in the above 23 cancer patient-derived colonocyte RNA samples and 7 healthy volunteer-derived colonocyte RNA samples are shown in Fig 4. In total, a high concordance was observed between the focused microarray and RT-PCR. The focused microarray detected 18 (78%) of the 23 cancer patients. Ten (71%) of the 14 early cancers (Dukes stage A or B) and 4 (80%) of the 5 right-sided cancers were detected.

Discussion

Although the number of samples examined in this study is considered to be small, the evidence suggests that these successful results could be obtained from the high-quality of the RNA of the colonocytes, which were isolated by FMCI. From a practical point of view for mass cancer screenings, it is noted that the same number of colonocytes from fecal

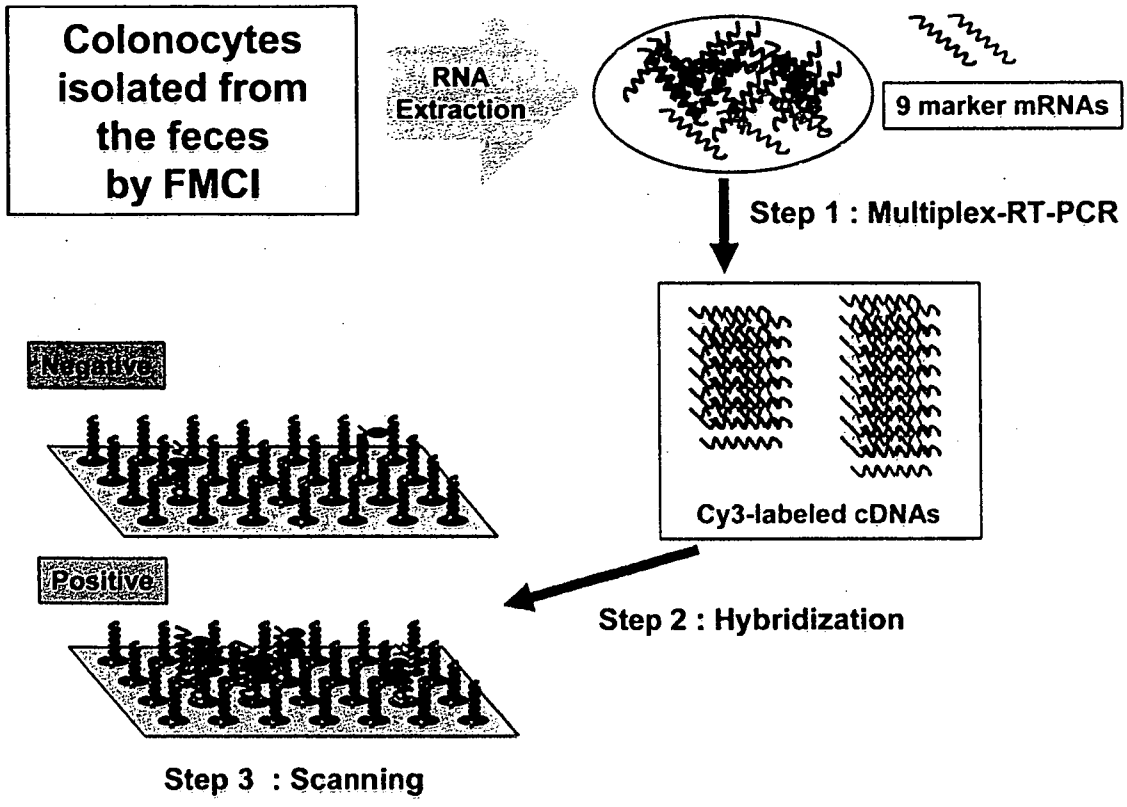

Figure 3. Schematic flow diagram of a focused micoarray assay. Marker mRNAs (PAP, REG1A, DPEP1, SEPP1, RPL27A, ATP1B1, EEF1A1, SFN, and RPS11 mRNAs) were amplified and labeled with Cy3-dUTP by multiplex-RT-PCR among total RNAs from colonocytes isolated by FMCI (step 1) and hybridized to focused micoarray (step 2), followed by fluorescence intensity scanning (step 3).

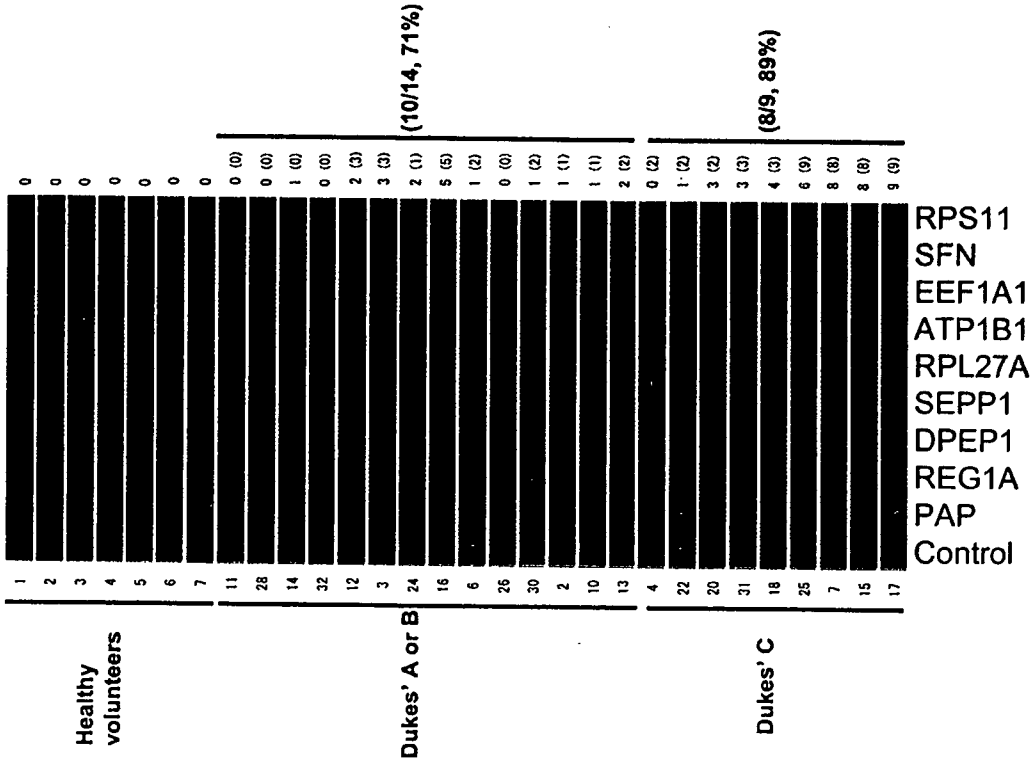

Figure 4. Hybridization image of focused microarray analysis and the number of positive genes in 30 colonocyte RNA samples. The Cy3-labeled cDNAs prepared by multiplex RT-PCR in two tubes were hybridized with 9 gene sequences (PAP, REG1A, DPEP1, SEPP1, RPL27A, ATP1B1, EEF1A1, SFN, and RPS11) on a focused microarray, which was manufactured by our previously developed Bubble Jet Technology with a small modification (25). Hybridization signals and the number of positive genes (right) in the above 23 cancer patient-derived colonocyte RNA samples and 7 healthy volunteer-derived colonocyte RNA samples are shown. In total, a high concordance was observed between focused microarray and RT-PCR. Ten (71%) of the 14 early cancers (Dukes stage A or B) and 8 (89%) of 9 Dukes stage C cancers were detected by the focused microarray analysis. The number of positive genes in RT-PCR are in parentheses (Fig. 2).

materials 6 h to 3 days after evacuation can be obtained if the feces are kept at 4°C (23). However, if conventional fecal RNA preparation methods without the epithelial cell enrichment process are used for colorectal cancer screening, we have to consider the contamination of blood in the feces, which derives from nonmalignant diseases. Considering the use of such methods, to this end we further provided 56 genes, which were expressed in the cancer patient-derived colonocytes but not in either the healthy volunteer-derived colonocytes or the peripheral blood mixture (Table II). This study suggests that the fecal RNA-based method could be a promising procedure for the detection of early or right-sided colorectal cancers. We recently developed a very effective focused microarray assay for detecting minimal gastric cancer cells in peritoneal washings, demonstrating a specificity and sensitivity equal to or better than cytology in two large specialist hospitals with trained cytologists (26). Therefore, the focused microarray assay could provide an effective imaging tool for mass screening, and our extensive gene list provides useful markers.

Acknowledgments

This study was supported in part by the program for promotion of Fundamental Studies in Health Sciences of the National Institute of Biomedical Innovation (NiBio); in part by a Grant-in-Aid for the Third Comprehensive 10-Year Strategy for Cancer Control and for Cancer Research (16-15) from the Ministry of Health, Labour and Welfare of Japan, and in part by a research and development project of the Industrial Science and Technology Program supported by the New Energy and Industrial Technology Development Organization (NEDO) of Japan. We thank Ayako Nomura and Megumi Sato for their excellent assistance with primer design for RT-PCR.

References

1. Mandel JS, Bond JH, Church TR, Snover DC, Bradley GM, Schman LM and Ederer F: Reducing mortality from colorectal cancer by screening for fecal occult blood. Minnesota Colon Cancer Control Study. N Engl J Med 328: 1365-1371, 1993.
2. Hardcastle JD, Chamberlain JO, Robinson MH, Moss SM, Amar SS, Balfour TW, James PD and Mangham CM: Randomised controlled trial of faecal-occult-blood screening for colorectal cancer. Lancet 348: 1472-1477, 1996.
3. Kronborg O, Fenger C, Olson J, Jorgensen OD and Sondergaard O: Randomized study of screening for colorectal cancer with faecal-occult-blood test. Lancet 348: 1467-1471, 1996.
4. Towler B, Irwig L, Glasziou P, Kewenter J, Weller D and Silagy C: A systematic review of the effects of screening for colorectal cancer using the faecal occult blood test, hemoccult. BMJ 317: 559-565, 1998.
5. Winawer S, Fletcher R, Rex D, Bond J, Burt R, Ferucci J, Ganiats T, Levin T, Woolf S, Johnson D, Kirk L, Litin S and Simmang C: Colorectal cancer screening and surveillance: clinical guidelines and rationale-update based on new evidence. Gastroenterology 124: 544-560, 2003.
6. Mandel JS, Church TR, Bond JH, Ederer F, Geisser MS, Mongin SJ, Snover DC and Schuman LM: The effect of fecal occult-blood screening on the incidence of colorectal cancer. N Engl J Med 343: 1603-1607, 2000.
7. Sidransky D, Tokino T, Hamilton SR, Kinzler KW, Levin B, Frost P and Vogelstein B: Identification of ras oncogene mutations in the stool of patients with curable colorectal tumors. Science 256: 102-105, 1992.
8. Hasegawa Y, Takeda S, Ichii S, Koizumi K, Maruyama M, Fujii A, Ohta H, Nakajima T, Okuda M, Baba S, *et al*: Detection of K-ras mutations in DNAs isolated from feces of patients with colorectal tumors by mutant-allele-specific amplification (MASA). Oncogene 10: 1441-1445, 1995.
9. Smith-Ravin J, England J, Talbot IC and Bodmer W: Detection of c-Ki-ras mutations in faecal samples from sporadic colorectal cancer patients. Gut 36: 81-86, 1995.
10. Eguchi S, Kohara N, Komuta K and Kanematsu T: Mutations of the p53 gene in the stool of patients with resectable colorectal cancer. Cancer 77: 1707-1710, 1996.
11. Nollau P, Moser C, Weinland G and Wagener C: Detection of K-ras mutations in stools of patients with colorectal cancer by mutant-enriched PCR. Int J Cancer 66: 332-336, 1996.
12. Ratto C, Flamini G, Sofo L, Nusera P, Ippliti M, Curigliano G, Ferreti G, Sgambato A, Merico M, Doglietto GB, Cittadini A and Crucitti F: Detection of oncogene mutation from neoplastic colonic cells exfoliated in feces. Dis Colon Rectum 39: 1238-1244, 1996.
13. Deuter R and Muller O: Detection of APC mutations in stool DNA of patients with colorectal cancer by HD-PCR. Hum Mutat 11: 84-89, 1998.
14. Ahlquist DA, Skoletsky JE, Boynton KA, Harrington JJ, Mahoney DW, Pierceall WE, Thibodeau SN and Shuber AP: Colorectal cancer screening by detection of altered human DNA in stool: feasibility of a multitarget assay panel. Gastroenterology 119: 1219-1227, 2000.
15. Dong SM, Traverso G, Johnson C, Geng L, Favis R, Boynton K, Hibi K, Goodman SN, D'Allessio M, Paty P, Hamilton SR, Sidransky D, Barany F, Levin B, Shuber A, Kinzler KW, Vogelstein B and Jen J: Detecting colorectal cancer in stool with the use of multiple genetic targets. J Natl Cancer Inst 93: 858-865, 2001.
16. Rengucci C, Maiolo P, Saragoni L, Zoli W, Amadori D and Calistri D: Multiple detection of genetic alterations in tumors and stool. Clin Cancer Res 7: 590-593, 2001.
17. Traverso G, Shuber A, Olsson L, Levin B, Johnson C, Hamilton SR, Boynton K, Kinzler KW and Vogelstein B: Detection of proximal colorectal cancers through analysis of faecal DNA. Lancet 359: 403-404, 2002.
18. Traverso G, Shuber A, Levin B, Levin B, Johnson C, Hamilton SR, Boynton K, Kinzler KW and Vogelstein B: Detection of APC mutations in fecal DNA from patients with colorectal tumors. N Engl J Med 346: 311-320, 2002.
19. Boynton KA, Summerhayes IC, Ahlquist DA and Shuber AP: DNA integrity as a potential marker for stool-based detection of colorectal cancer. Clin Chem 49: 1058-1065, 2003.
20. Matsumura Y and Tarin D: Significance of CD44 gene products for cancer diagnosis and disease evaluation. Lancet 340: 1053-1058, 1992.
21. Mastumura Y, Hanbury D, Smith J and Tarin D: Non-invasive detection of malignancy by identification of unusual CD44 gene activity in exfoliated cancer cells. BMJ 308: 619-624, 1994.
22. Yamao T, Matsumura Y, Shimada Y, Moriya Y, Sugihara K, Akasu T, Fujita S and Kakizoe T: Abnormal expression of CD44 variants in the exfoliated cells in the feces of patients with colorectal cancer. Gastroenterology 114: 1196-1205, 1998.
23. Matsushita H, Matsumura Y, Moriya Y, Akasu T, Fujita S, Yamamoto S, Onouchi S, Saito N, Sugito M, Ito M, Kozu T, Minowa T, Nomura S, Tsunoda H and Kakizoe T: A new method for isolating colonocytes from naturally evacuated feces and its clinical application to colorectal cancer diagnosis. Gastroenterology 129: 1918-1927, 2005.
24. Mori K, Aoyagi K, Ueda T, Danjoh I, Tsubosa Y, Yanagihara K, Matsuno Y, Sasako M, Sakamoto H, Mafune K, Kaminishi M, Yoshida T, Terada M and Sasaki H: Highly specific marker genes for detecting minimal gastric cancer cells in cytology negative peritoneal washings. Biochem Biophys Res Commun 313: 931-937, 2004.
25. Okamoto T, Suzuki T and Yamamoto N: Microarray fabrication with covalent attachment of DNA using Bubble Jet Technology. Nat Biotech 18: 438-441, 2000.
26. Mori K, Suzuki T, Uozaki H, Nakanishi H, Ueda T, Matsuno Y, Kodera Y, Sakamoto H, Yamamoto N, Sasako M, Kaminishi M and Sasaki H: Detection of minimal gastric cancer cells in peritoneal washings by focused microarray analysis with multiple markers: clinical implications. Ann Surg Oncol 14: 1694-1702, 2007.

Available online at www.sciencedirect.com
ScienceDirect
Journal of Controlled Release 117 (2007) 267–272
journal of controlled release
www.elsevier.com/locate/jconrel
GENE DELIVERY

Spinal gene transfer using ultrasound and microbubbles

Masahiko Takahashi [a,*], Kanta Kido [a], Atsuko Aoi [a,b], Hiroshi Furukawa [c], Masao Ono [c], Tetsuya Kodama [b]

[a] Department of Oral Medicine and Surgery, Tohoku University Graduate School of Dentistry, Japan
[b] Department of Nanomedicine, Tohoku University Biomedical Engineering Research Organization, Japan
[c] Department of Pathology, Tohoku University Graduate School of Medicine, Japan

Received 19 June 2006; accepted 24 October 2006
Available online 6 November 2006

Abstract

Spinal gene therapy is a promising option for treating various spinal-related disorders. Several previous studies using viral vectors reported successful transfer of therapeutic genes into the spinal nerve system. However, because of the considerable immunogenicity related to the use of viruses, non-viral gene transfer still needs to be developed. One possible approach is the combined use of ultrasound and echo-contrast microbubbles. The present study shows that this method can be applied for targeted intrathecal gene delivery. We intrathecally injected a mixture of plasmid-DNA encoded with luciferase and commercially available albumin microbubbles by needle puncture at the lower lumbar intervertebral space in mice. Subsequent percutaneous ultrasonication on the lumbar vertebrae significantly enhanced the luciferase expression, analyzed by imaging luciferin bioluminescence, in the dorsal meningeal cells at the insonated region. No apparent neurological damages were induced by the present spinal interventions. In addition to the general benefits of the combined use of ultrasound and microbubbles, our approach can offer some advantages specific to spinal gene transfection including minimal invasiveness of simple percutaneous dural puncture, targetability due to the limited access of ultrasound waves through anatomical apertures of the vertebrae, and possible paracrine delivery of therapeutic molecules to the spinal nerve system.

Keywords: Gene therapy; Spinal disorder; Intrathecal delivery; Ultrasound; Microbubble

1. Introduction

Spinal gene transfer is expected to become a promising option for treating various spinal-related disorders including nerve injury, degenerative diseases, neoplasm, and chronic pain [1,2]. To date, the most widely used vehicles for gene delivery are viral vectors. Recent animal studies using adenovirus vectors indicated that direct spinal injection of specific growth-factor genes achieved functional recovery after acute spinal cord injury [3–5]. The feasibility of virus-mediated gene transfer to treat chronic pain has been also explored using the precursor genes of endogenous opioids [6,7]. The targeted spinal tissues for the opioid-gene transfer can be both meningeal and parenchyma cells. Among the utilized viral vectors that are mostly derived either from adenoviruses, adeno-associated viruses, herpes simplex viruses or retroviruses [8], herpes vectors may be the most promising for antinociceptive gene therapy because of its high selectivity to primary afferent neurons [2,9].

Despite such experimental successes in virus-mediated gene delivery, however, alternative non-viral transgene applications need to be developed because the clinical use of viral vectors is limited by such possible disadvantages as immunogenic properties, inflammatory responses, and the difficulty of producing large amounts of pure virus. In this context, it has been reported recently that the emission of high-pressure ultrasound in combination with echo-contrast agents, microbubbles, can facilitate gene transfection into cells [10]. Possible explanations for the mechanisms include the production of transient pores on the cell membranes as well as an increase in the

* Corresponding author. Division of Dento-oral Anesthesiology, Department of Oral Medicine and Surgery, Tohoku University Graduate School of Dentistry, 4-1 Seiryo-machi, Aoba-ku, Sendai 980-8575, Japan. Tel./fax: +81 22 717 8401.
E-mail address: m-takaha@mail.tains.tohoku.ac.jp (M. Takahashi).

0168-3659/$ - see front matter © 2006 Elsevier B.V. All rights reserved.
doi:10.1016/j.jconrel.2006.10.026

membrane fluidity by impulsive pressures raised when microbubbles are disrupted by ultrasound [11,12]. The combined use of microbubbles and ultrasound for gene delivery has several advantages including low toxicity, low immunogenicity, low invasiveness, high target selectivity, and repeatable applicability [11]. In the present study, we focused on spinal gene delivery and demonstrated that percutaneous ultrasonication in combination with intrathecal microbubbles facilitated gene transfection in spinal meningeal cells in mice.

2. Materials and methods

2.1. Animals

The study was approved by the Animal Care Committee of Tohoku University Graduate School of Medicine. Male inbred BALB/c mice were purchased from the institutional breeding facilities at 5–6 weeks of age and maintained in an antigen- and virus-free room (22 ± 1 °C, 60 ± 10% relative humidity, 12 h/12 h light/dark cycle, food and water *ad libitum*). The mice were studied at 7–8 weeks of age.

2.2. Plasmid DNA

pCMV-luciferase-GL3 (pcLuc-GL3: 7.4 kb) was constructed by cloning the luciferase gene from the pGL3-Control Vector (Promega Corp., Madison, WI, USA) into pcDNA3 (5.4 kb) (Invitrogen, San Diego, CA, USA) at the *Hin*dIII and *Bam*HI sites. Plasmid DNA was purified with a QIAGEN plasmid isolation kit (QIAGEN, Hilden, Germany) and prepared at a final concentration of 1 mg/ml.

2.3. Intrathecal transfection of plasmid DNA

Mice were anesthetized with an intraperitoneal injection of sodium pentobarbital (80 mg/kg) and immobilized in a prone position on an acrylic plate. Intrathecal access was accomplished by percutaneous lumbar puncture through the 4/5th or 5/6th intervertebral space using a 27-gauge stainless-steel needle according to the Hylden and Wilcox technique with modification [13]. Dural penetration of the needle was confirmed by inspecting tail flicks of the mice. A total volume of 10 μl containing 5 μg plasmid and commercially available albumin-coated octa-fluoropropane gas microbubbles (MB), Optison™ (Amersham Health, Oslo, Norway; $5–8 \times 10^8$/ml, 3–4.5 μm in diameter), in phosphate buffered saline at a final MB concentration either 0, 20, or 50 v/v% was then injected slowly into the intrathecal space using a 50-μl microsyringe (Hamilton, Bonaduz, GR, Switzerland). A mixture of the plasmid with MB was prepared by gentle hand shaking immediately before injection. Immediately after the intrathecal injection, the mice were placed at a vertical position in a 37 °C water bath and dorsally insonated for 1 min at the vertebral region that had been injected using an ultrasound-emitting transducer (6 mm in diameter; Fuji Ceramics Co., Fujinomiya, Japan). The ultrasound (US) parameters used were as follows: central frequency, 950 kHz; duty ratio, 20%; the average intensity per cross section, 1.3 W/cm^2; acoustic pressure at a standoff distance of 1 mm from the transducer surface, 0.6 MPa; energy, 2.4 J/cm^2. After the insonation, the mice were dried and kept under a heat lamp until recovery from anesthesia.

2.4. Analysis of luciferase activity

Mice were killed by neck dislocation under deep anesthesia with isoflurane at 1, 3, 7 days after transfection of the luciferase gene. The spinal cord was harvested *en bloc* at the level of the lower thoracic to sacral region by careful dissection of the vertebrae and placed on a dish plate. Subsequently, the tissue was fully covered with Luciferin 30 mg in 1 ml PBS (Promega Co., Madison, WI, USA). Luciferin bioluminescence was immediately quantified as the luciferase activity using an *in vivo* imaging system (IVIS™, Xenogen Co., Alameda, CA, USA) [14].

2.5. Immunohistochemistry

The harvested spinal cords were preserved in 10% PFA for 4 h and then embedded in paraffin and sectioned. Sections (4 μm thickness) were evaluated for the presence of luciferase protein by immunostaining. The sections were deparaffinized in xylene for 5 min 3×, rehydrated through graded ethanol and equilibrated in PBS. The sections were incubated in 3% H_2O_2 for 30 min to dampen endogenous peroxidase activity. They were incubated for 30 min at room temperature with 10% normal goat serum (Nichirei Biosciences Inc., Tokyo) to reduce nonspecific protein binding. After a wash in PBS, the sections were incubated with biotin-labeled rabbit anti-luciferase antibody (0.5 g/ml) (Cortex Biochem, San Leandro, CA, USA) overnight at 4 °C. The following day, after three washes in PBS, immunoreactivity was detected using an anti-rabbit IgG Histofine SAB-PO(M) kit (Nichirei Biosciences Inc., Tokyo, Japan) and diaminobenzidine (DAB) as a chromogen according to the manufacturer's protocols. After color development, the spinal cord sections were counterstained with hematoxylin and were then dehydrated, cleared, and mounted on slides.

2.6. Assessment of post-transfectional spinal injury

2.6.1. Thermal nociception

For assessing the nociceptive responses to thermal stimuli after the intrathecal procedure, the paw withdrawal latencies following exposure to infra-red radiant heat were determined [15] using a commercial device (7370-Planter Test, Ugo Basille, Comerio, Italy) three days after the gene transfection. Mice were placed in a clear plastic chamber (210 mm × 105 mm × 130 mm) with a glass floor and allowed to acclimate for at least 5 min. After the acclimation period, radiant heat was projected to the hind paw and time count was started. The heat projection was made through a 5 mm × 10 mm aperture in the top of a movable case containing the radiant heat source that was positioned under the glass floor directly beneath the paw. The radiant heat source consisted of a high intensity projecting Halogen lamp bulb (8 V–50 W) located 40 mm below the floor. The time count was stopped when the mouse withdrew its paw. Mice were tested

with three determinations each at the right and left paw and were allowed to rest for at least 30 min between each session.

2.6.2. Rotarod

For assessing motor function after the intrathecal procedure, mice were tested using a rotarod (IITC; Life Science Instrument, Woodland Hills, CA, USA) three days after the gene transfection. The rod had a diameter of 3.8 cm and was accelerated from 0 to 30 rpm over a 17.5-s period. The total time that the mice remained on the rotarod was measured. The time count was stopped when mice fell from the rod or when they rotated around completely two times without walking [16]. Mice were tested with three trials and were allowed to rest for at least 30 min between each session.

2.7. Statistical analysis

All values are expressed as mean±SEM. Statistical analysis for the spinal luciferase activities was performed by one-factor analysis of variance (ANOVA) with Fisher's protected least significant difference test (Fisher's PLSD) as a post-hoc procedure. Unpaired Student-T test was used for the behavioral evaluations. Statistical significance was defined as $p<0.05$.

3. Results

3.1. Effects of microbubbles and ultrasound on spinal gene transfection

Fig. 1 shows representative views of luciferin bioluminescence in the mouse spinal cord obtained by the imaging system (sum of photon counts from a region of interest at 5 min is presented). The spinal luciferase activities determined one day after four different treatments (DNA alone, DNA+MB, DNA+US, and DNA+MB+US) are shown in Fig. 2a. The concentration of MB used was 50%. The luciferase activities in the treatments with DNA+MB and DNA+US were as low as that with DNA alone. In contrast, ultrasonication after the DNA+MB injection significantly increased the luciferase activity by approximately 25 fold compared to the other treatments ($p<0.001$).

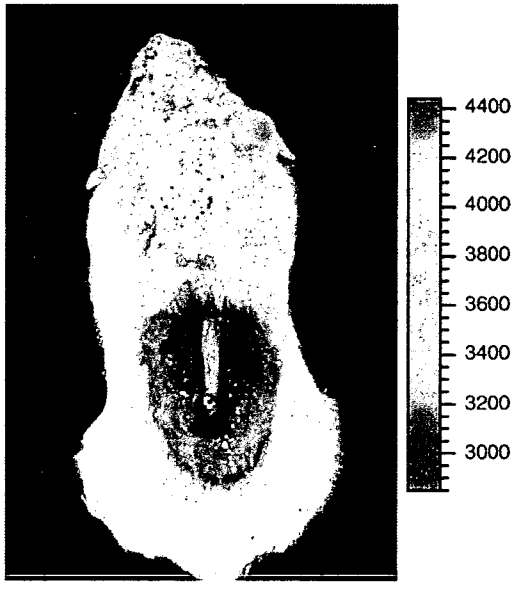

Fig. 1. Representative image showing luciferin bioluminescence (IVIS™, Xenogen Co., Alameda, CA, USA) in the spinal cord of BALB/c mice a day after the intrathecal injection of plasmid DNA and microbubbles (Optison™, Amersham Health, Oslo, Norway) followed by percutaneous ultrasonication. Imaging time is 5 min. Color bar units represent photons s^{-1} cm^{-2}.

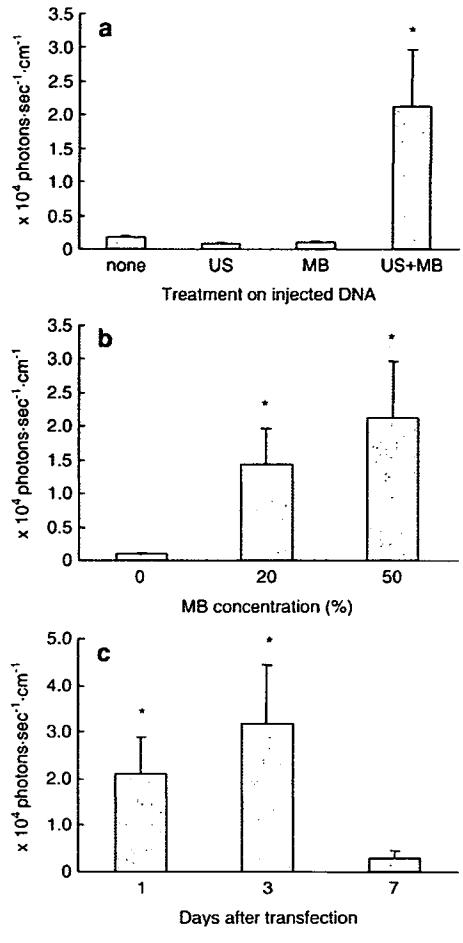

Fig. 2. Plasmid-derived spinal luciferase activity represented by luciferin bioluminescence in mice subjected to intrathecal gene delivery using ultrasound and microbubbles. The ultrasound parameters were as follows: central frequency, 950 kHz; duty ratio, 20%; the average intensity per cross section, 1.3 W/cm^2; acoustic pressure at a standoff distance of 1-mm from the transducer surface, 0.6 MPa; energy, 2.4 J/cm^2; exposure time, 1 min. (a) Treatment effects of ultrasound and 50% microbubbles one day after the application. Combined use of ultrasound and microbubbles significantly enhanced the gene transfection compared to the other treatments. (b) Effects of the microbubble concentration on the spinal gene expression. Microbubbles at concentrations of both 20 and 50% significantly enhanced the gene transfection one day after the application. No significant difference was found between the luciferase activities in mice treated with the two concentrations. (c) Time course of spinal gene expression in mice treated with ultrasound and 50% microbubbles. Luciferase activity significantly increased at 1 and 3 days after gene transfection which disappeared by the 7th day. No statistical difference was found between the gene expression at 1 and 3 days post-transfection. *$p<0.001$. $n=5$ in each group. US: ultrasound; MB: microbubble (Optison).

3.2. Effects of microbubble concentration on spinal gene transfection

Fig. 2b shows the spinal luciferase activities one day after ultrasonication with 0, 20, and 50% MB. While the treatment with MB significantly increased the luciferase activities ($p<0.02$), the difference between 20 and 50% MB was not significant.

3.3. Time course of spinal gene expression

The spinal luciferase activities were analyzed at 1, 3, and 7 days after the intrathecal gene transfection using US and 50% MB (Fig. 2c). The luciferase activities significantly increased at 1 and 3 days post-transfection ($p<0.02$) without an intergroup difference, and returned to a level similar to that without US (at 1 day post-treatment) after 7 days.

3.4. Histological localization of the transfected gene expression

The immunohistochemical staining revealed that luciferase expression was mostly limited to the meningeal cells in the dorsal surface of the spinal cord (Fig. 3). The expressing regions were likely to have been the dura mater because Fig. 3b clearly shows a positive staining for cells in a membrane structure apart from the spinal parenchyma by the space of medullary fluid. As the dura mater consists of two cell types, meningeal cell and endothelial cell, the present data cannot strictly exclude the positive staining for the endothelial cells. However, the endothelial cells are shown to be very minor cellular component, so that frequent staining may indicate expression of the gene product mainly in the meningeal cells. There were no hemorrhage or inflammatory findings in the sections.

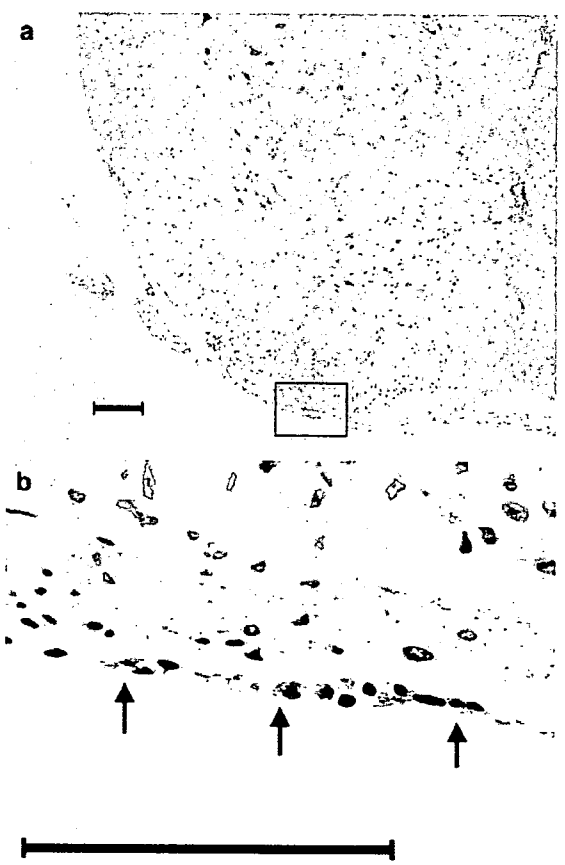

Fig. 3. Local gene expression in mouse spinal cord after intrathecal gene delivery using ultrasound and microbubbles. Expression of luciferase protein was mostly limited to the dorsal meningeal cells. (a) H&E staining in coronal sections of the lumber spinal cord. (b) Immunohistochemical localization of luciferase (arrows). Scale bar = 100 μm.

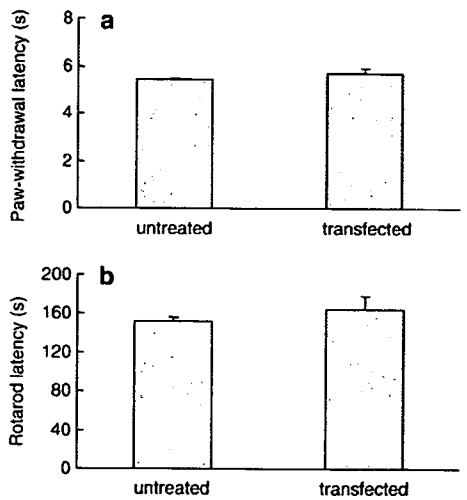

Fig. 4. Neurological evaluations of mice obtained 3 days after gene transfection using ultrasound and microbubbles (50%). (a) Paw-withdrawal latency following exposure to infra-red radiant heat. Three determinations each in the right and left hind paw were combined in each animal because the latency did not differ between the two sides. (b) Rotarod latency that represents the total time mice remained on the rotarod. Each mouse was tested with three trials. No significant difference was found compared to untreated mice in either determination. $n=4$ in each group. US: ultrasound; MB: microbubble (Optison).

3.5. Paw-withdrawal and rotarod latencies

Fig. 4 shows the averaged paw-withdrawal (Fig. 4a) and rotarod latencies (Fig. 4b) in untreated and transfected (DNA + 50% MB + US) mice. Since the withdrawal latencies were not different between the right and left paw (data not shown), the data were combined in each animal. The determinations revealed no significant difference in the paw-withdrawal or rotarod latencies between the two groups, indicating that the present intervention did not affect the sensory and motor neurologic functions of the mice.

4. Discussion

The present study clearly demonstrated that percutaneous ultrasonication on an intrathecally administered mixture of plasmid-DNA and Optison facilitated the transfection of luciferase genes into the spinal meningeal cells in mice. No significant deficit was observed either in the sensory or motor neurologic functions after the procedures. In addition to the

general benefits of the combined use of ultrasound and microbubbles, our approach offers some advantages specific to spinal gene transfection. First, it requires only intrathecal needle access and percutaneous sonication that have been widely accepted in the clinical practice. Although a relatively short duration of gene expression (<7 days) was observed (Fig. 2c), the minimal invasiveness of the present surgical interventions would permit repetitive gene delivery into the spinal cord. Second, the intervertebral foramina and spaces would provide highly selective anatomical windows for ultrasound access while the vertebral bony structures would protect the spinal cord from possible excessive sonication. Although spotty gene expressions in the insonated regions would not be obvious in animals as small as the mice used in this study (Fig. 1), it can be expected that an ultrasound beam could reach the regions of the dorsal roots or the dorsal horns at targeted vertebral levels through the boneless apertures in large animals including human. This can be especially promising for transferring antinociceptive genes. Third, gene transfer into meningeal cells (Fig. 3) may be useful for topical delivery of bioactive substances into the CSF or adjacent spinal parenchyma while avoiding direct genetic modulation of parenchyma cells. Transgene-derived peptides such as growth factors, neuropeptides, or endogenous opioids that are secreted from meningeal cells would act in a paracrine manner on neurons and glias in the near vicinity, circumventing pharmacological problems related to the short half-life of the peptides or the need for high doses to achieve biological activity that could result in undesirable side effects.

Spinal gene therapy can be expected to be a promising approach to treat various spinal-related disorders. In previous animal studies, the delivery of therapeutic genes into the spinal nerve system has been mostly achieved using viral vectors [8]. However, because of the considerable disadvantages involved in using viral vectors, the development of alternative non-viral transgene techniques is needed. Cationic reagents such as cationic liposomes [17] have been developed for non-viral gene transfection. Achieving the efficient delivery of such molecules, however, to the spinal cord includes inherent difficulties. First, intrathecal injection induces diffusion of reagents into the cerebral spinal fluid (CSF), resulting in lack of target specificity. Second, since the CSF continuously circulates and replaces, a constant concentration of reagents for necessary transfection to a specific site would not be achieved. Ultrasound gene therapy is an alternative non-viral approach [18]. The insufficient transfection efficiency of simple ultrasonication can be improved by the combined use of echo-contrast microbubbles [11]. The use of ultrasound with microbubbles, which enables non-invasive, tissue-specific gene delivery, has received much interest and enhanced gene transfer has been reported in various animal tissues *in vivo* including heart [19], peripheral arteries [20], skeletal muscles [21], and brain [22]. Very recently, Shimamura et al. reported successful gene transfer into the rat spinal cord using ultrasound and microbubbles [23]. The authors intrathecally injected naked luciferase DNA with Optison through the 4/5th lumbar intervertebral space and applied sonication directly on the thoracic dural sac by removing the dorsal part of the 9–10th thoracic vertebra, which resulted in the enhanced expression of luciferase in the meningeal cells in the insonated region. In contrast, we accomplished transgene expression in the meningeal cells by intrathecal injection of luciferase DNA with Optison through the lower lumbar intervertebral space, as in their study, but then employed simple transcutaneous insonation at the same lumbar region without surgical exposure of the dura. The lower invasiveness in our methodology would seem to be more clinically useful. Interestingly, the duration of transgene expression was consistently as short as a week in both studies. Although Shimamura et al. described that the short expression of transgene by single transfection would be acceptable to treat acute spinal cord trauma [23], the repeated applicability due to the lower invasiveness in the present study could enable treatments for chronic ailments. In fact, we have recently shown that successive gene expression was obtained by repeat transfection using the present ultrasound–microbubble technique [24]. Nonetheless, since gene expression for longer than 3 weeks was previously achieved by spinal electroporation via an intrathecal electrode catheter in rat meningeal cells [25,26], the present ultrasound–microbubble approach has the potential for methodological improvement to prolong the duration of transgene expression by optimizing acoustic parameters such as intensity, duty ratio, frequency, and spatial pressure distribution [12] and changing the membrane properties of microbubbles [27].

The present acoustic parameters were relatively consistent with those reported in previous studies in which ultrasound and Optison were safely used for transferring genes into nervous tissues [22,23]. Consistent with those studies, we did not find macroscopic injuries in the skin or muscles, microscopic damage in the spinal cord, or significant deficits in the spinal neurological functions. In addition, the present neurological tolerance may be alternatively explained by a characteristic of our approach, namely that the intact vertebral bony structures surrounding the intervertebral apertures limited excessive sonication of the spinal cord. Nonetheless, further optimization of the ultrasound parameters will improve the safeness of sonication on nervous tissues. The physical conditions of the microbubbles used in this study are additional issues to be discussed. First, although we evaluated only the usefulness of Optison, the possible utility and safety of microbubbles other than Optison (e.g. lipid microbubbles) for intrathecal gene transfer remains to be explored. Second, we should note that Optison at a concentration as high as 50% was used in most series of the present experiments. The reasons for this were that a trend of higher transfection efficacy was observed in the 50% group (but ns vs. 20% groups, Fig. 2b) and that no apparent neurological damage was observed in the transfected mice (Fig. 4). However, earlier studies [22,23] successfully used Optison at concentrations of 20–25% for intrathecal gene delivery in rats. It seems reasonable that intrathecal microbubbles at lower concentrations would induce fewer adverse effects while enabling an increase in the relative content of plasmid DNA in a limited volume of mixture. Therefore, it is possible that the concentration of microbubbles for intrathecal injection could be further optimized. The authors finally note

that the functional expressions of genes transfected into the spinal nerve system have not yet been examined. Further efforts using genes that are encoded with neurobioactive peptides are clearly needed to investigate the clinical usefulness of the present ultrasound–microbubble approach.

In conclusion, we demonstrated that simple percutaneous ultrasonication on intrathecally administered plasmid DNA and echo-contrast microbubbles enhanced the gene transfer into spinal meningeal cells in mice. The present approach can provide some advantages specific to spinal gene therapy including minimal invasiveness, regional targetability, and possible paracrine delivery of therapeutic molecules to the spinal nerve system. Studies including functional assessments of therapeutic gene transfer as well as the application of the techniques in larger animals will further clarify the feasibility of the present ultrasound–microbubble method in spinal gene therapy.

References

[1] J.C. Glorioso, D.J. Fink, Herpes vector-mediated gene transfer in treatment of diseases of the nervous system, Annu. Rev. Microbiol. 58 (1) (2004) 253–271.

[2] S.P. Wilson, Gene-based therapy for treatment of chronic pain, Semin. Pain Med. 1 (4) (2003) 220–226.

[3] F. Facchiano, E. Fernandez, S. Mancarella, G. Maira, M. Miscusi, D. D'Arcangelo, G. Cimino-Reale, M.L. Falchetti, M.C. Capogrossi, R. Pallini, Promotion of regeneration of corticospinal tract axons in rats with recombinant vascular endothelial growth factor alone and combined with adenovirus coding for this factor, J. Neurosurg. 97 (1) (2002) 161–168.

[4] M. Koda, M. Hashimoto, M. Murakami, K. Yoshinaga, O. Ikeda, M. Yamazaki, S. Koshizuka, T. Kamada, H. Moriya, H. Shirasawa, S. Sakao, H. Ino, Adenovirus vector-mediated in vivo gene transfer of brain-derived neurotrophic factor (BDNF) promotes rubrospinal axonal regeneration and functional recovery after complete transection of the adult rat spinal cord, J. Neurotrauma 21 (3) (2004) 329–337.

[5] X.Q. Tang, Y. Wang, Z.H. Huang, J.S. Han, Y. Wan, Adenovirus-mediated delivery of GDNF ameliorates corticospinal neuronal atrophy and motor function deficits in rats with spinal cord injury, NeuroReport 15 (3) (2004) 425–429.

[6] S.P. Wilson, D.C. Yeomans, M.A. Bender, Y. Lu, W.F. Goins, J.C. Glorioso, Antihyperalgesic effects of infection with a preproenkephalin-encoding herpes virus, Proc. Natl. Acad. Sci. U. S. A. 96 (6) (1999) 3211–3216.

[7] A.A. Finegold, A.J. Mannes, M.J. Iadarola, A paracrine paradigm for in vivo gene therapy in the central nervous system: treatment of chronic pain, Hum. Gene Ther. 10 (7) (1999) 1251–1257.

[8] M. Pohl, J. Braz, Gene therapy of pain: emerging strategies and future directions, Eur. J. Pharmacol. 429 (1–3) (2001) 39–48.

[9] M. Mata, J. Glorioso, D.J. Fink, Development of HSV-mediated gene transfer for the treatment of chronic pain, Exp. Neurol. 184 (Suppl. 1) (2003) S25–S29.

[10] P.A. Dijkmans, L.J.M. Juffermans, R.J.P. Musters, A. van Wamel, F.J. ten Cate, W. van Gilst, C.A. Visser, N. de Jong, O. Kamp, Microbubbles and ultrasound: from diagnosis to therapy, Eur. J. Echocardiog. 5 (4) (2004) 245–256.

[11] R. Bekeredjian, P.A. Grayburn, R.V. Shohet, Use of ultrasound contrast agents for gene or drug delivery in cardiovascular medicine, J. Am. Coll. Cardiol. 45 (3) (2005) 329–335.

[12] T. Kodama, Y. Tomita, K. Koshiyama, M.J.K. Blomley, Transfection effect of microbubbles on cells in superposed ultrasound waves and behavior of cavitation bubble, Ultrasound Med. Biol. 32 (6) (2006) 905–914.

[13] J.L. Hylden, G.L. Wilcox, Intrathecal morphine in mice: a new technique, Eur. J. Pharmacol. 67 (2–3) (1980) 313–316.

[14] B.W. Rice, M.D. Cable, M.B. Nelson, In vivo imaging of light-emitting probes, J. Biomed. Opt. 6 (4) (2001) 432–440.

[15] K.M. Hargreaves, R. Dubner, F. Brown, C. Flores, J. Joris, A new and sensitive method for measuring thermal nociception in cutaneous hyperalgesia, Pain 32 (1) (1988) 77–88.

[16] J.D. Hommel, R.M. Sears, D. Georgescu, D.L. Simmons, R.J. DiLeone, Local gene knockdown in the brain using viral-mediated RNA interference, Nat. Med. 9 (12) (2003) 1539–1544.

[17] C.R. Dass, P.F. Choong, Selective gene delivery for cancer therapy using cationic liposomes: in vivo proof of applicability, J. Control. Release 113 (2) (2006) 155–163.

[18] C.M. Newman, A. Lawrie, A.F. Brisken, D.C. Cumberland, Ultrasound gene therapy: on the road from concept to reality, Echocardiography 18 (4) (2001) 339–347.

[19] R. Bekeredjian, S. Chen, P.A. Frenkel, P.A. Grayburn, R.V. Shohet, Ultrasound-targeted microbubble destruction can repeatedly direct highly specific plasmid expression to the heart, Circulation 108 (8) (2003) 1022–1026.

[20] Y. Taniyama, K. Tachibana, K. Hiraoka, T. Namba, K. Yamasaki, N. Hashiya, M. Aoki, T. Ogihara, K. Yasufumi, R. Morishita, Local delivery of plasmid DNA into rat carotid artery using ultrasound, Circulation 105 (10) (2002) 1233–1239.

[21] Y. Taniyama, K. Tachibana, K. Hiraoka, M. Aoki, S. Yamamoto, K. Matsumoto, T. Nakamura, T. Ogihara, Y. Kaneda, R. Morishita, Development of safe and efficient novel nonviral gene transfer using ultrasound: enhancement of transfection efficiency of naked plasmid DNA in skeletal muscle, Gene Ther. 9 (6) (2002) 372–380.

[22] M. Shimamura, N. Sato, Y. Taniyama, M. Endo, H. Kurinami, M. Aoki, T. Ogihara, Y. Kaneda, R. Morishita, Development of efficient plasmid DNA transfer into adult rat central nervous system using microbubble-enhanced ultrasound, Gene Ther. 11 (20) (2004) 1532–1539.

[23] M. Shimamura, N. Sato, Y. Taniyama, H. Kurinami, H. Tanaka, T. Takami, M. Ogihara, Y. Tohyama, R. Morishita, Gene transfer into adult rat spinal cord using naked DNA and ultrasound microbubbles, J. Gene Med. 7 (11) (2005) 1468–1474.

[24] A. Aoi, K. Konno, S. Fumiaki, S. Mori, G. Vassaux, T. Kodama, HSV-tk/GCV cytotoxic gene therapy using ultrasound and nanobubbles, Ultrasound Med. Biol. 32 (5S) (2006) 280.

[25] C.R. Lin, M.H. Tai, J.T. Cheng, A.K. Chou, J.J. Wang, P.H. Tan, M. Marsala, L.C. Yang, Electroporation for direct spinal gene transfer in rats, Neurosci. Lett. 317 (1) (2002) 1–4.

[26] T.H. Lee, L.C. Yang, A.K. Chou, P.C. Wu, C.R. Lin, C.H. Wang, J.T. Chen, C.S. Tang, In vivo electroporation of proopiomelanocortin induces analgesia in a formalin-injection pain model in rats, Pain 104 (1–2) (2003) 159–167.

[27] J.R. Lindner, Microbubbles in medical imaging: current applications and future directions, Nat. Rev. Drug Discov. 3 (6) (2004) 527–532.

Journal of Drug Targeting, August–September 2007; 15(7–8): 507–517

informa
healthcare

Preclinical and clinical studies of anticancer drug-incorporated polymeric micelles

YASUHIRO MATSUMURA

Investigative Treatment Division, Research Center for Innovative Oncology, National Cancer Center Hospital East, Kashiwa, Chiba, Japan

Abstract

Tumour-targeted delivery of therapeutic agents is a longstanding pharmacological goal to improve selectivity and Therapeutic Index. Most scientists have sought to use 'active' receptor-mediated tumour-targeting systems, however the 'passive' targeting afforded by the Enhanced Permeability and Retention (EPR) effects provides a versatile and non-saturable opportunity for tumour-selective delivery. Polymeric micelles are ideally suited to exploit the EPR effect, and they have been used for the delivery of a range of anticancer drugs in preclinical and clinical studies. Here I overview some of the more important approaches, assessing usefulness and seeking to identify the most promising ways to apply the phenomenon of passive targeting for improved clinical outcome.

Keywords: *Micelles, anticancer agent, EPR effect, clinical trial*

Preface

Several problems of anticancer agents are recognized, such as their low therapeutic indices and limited efficacy due to the nonselective nature of their therapeutic targets and their inability to accumulate selectively in cancer tissues. Therefore, it would be desirable to develop modalities by which cytotoxic drugs can be selectively targeted to tumour tissues and allowed to act effectively on only the cancer cells in the tumor. The role of drug delivery systems (DDS) has drawn attention in this context. DDS could be used for active or passive targeting of tumor tissues. The former refers to the development of monoclonal antibodies directed against tumour-related molecules that allow targeting of the tumour, because of specific binding between the antibody and its antigen. However, the application of DDS using monoclonal antibodies is restricted to tumours expressing high levels of related antigens.

About a quarter of a century ago, after training as a surgeon, I started my career in the field of DDS under the supervision of Prof. Maeda. We made intensive efforts to ascertain the mechanism of accumulation of macromolecules in solid tumours. Finally, we succeeded in publishing the first paper, in 1986, on the enhanced permeability and retention (EPR) effect (Matsumura and Maeda 1986). Passive targeting is based on this EPR effect. The EPR effect is based on the pathophysiological characteristics of solid tumour tissues: hypervascularity, incomplete vascular architecture, secretion of vascular permeability factors stimulating extravasation within cancer tissue, and absence of effective lymphatic drainage from tumours that impedes the efficient clearance of macromolecules accumulated in solid tumour tissues.

Several techniques to maximally use the EPR effect have been developed, e.g. modification of drug structures and development of drug carriers. Polymeric micelle-based anticancer drugs were originally developed by Prof. Kataoka et al. in late the 1980's or early 1990's (Yokoyama et al. 1990; 1991a, b, c; Kataoka et al. 1993). Polymeric micelles were expected to increase the accumulation of drugs in tumour tissues utilizing the EPR effect and to incorporate various kinds of drugs into the inner core by chemical conjugation or physical entrapment with relatively high stability. The size of the micelles

Correspondence: Y. Matsumura, Investigative Treatment Division, Research Center for Innovative Oncology, National Cancer Center Hospital East, Kashiwa, Chiba, Japan.

ISSN 1061-186X print/ISSN 1029-2330 online
DOI: 10.1080/10611860701499888

can be controlled within the diameter range of 20–100 nm, to ensure that the micelles do not pass through normal vessel walls; therefore, a reduced incidence of the side effects of the drugs may be expected due to the decreased volume of distribution.

In this chapter, polymeric micelle systems for which clinical trials are now underway are reviewed.

NK105, paclitaxel-incorporating micellar nanoparticle

Paclitaxel (PTX) is one of the most useful anticancer agents known for various cancers, including ovarian, breast and lung cancers (Carney 1996; Khayat et al. 2000). However, PTX has serious adverse effects, e.g. neutropenia and peripheral sensory neuropathy. In addition, anaphylaxis and other severe hypersensitive reactions have been reported to develop in 2–4% of patients receiving the drug even after premedication with antiallergic agents; these adverse reactions have been attributed to the mixture of Cremophor EL and ethanol which was used to solubilize PTX (Weiss et al. 1990; Rowinsky and Donehower 2003). Of the adverse reactions, neutropenia can be prevented or managed effectively by administering a granulocyte colony-stimulating factor. On the other hand, there are no effective therapies to prevent or reduce nerve damage which is associated with peripheral neuropathy caused by PTX; therefore, neurotoxicity constitutes a significant dose-limiting toxicity (DLT) of the drug (Rowinsky et al. 1993; Wasserheit et al. 1996).

Preparation and characterization of NK105

To construct NK105 micellar nanoparticles (Figure 1), block copolymers consisting of polyethylene glycol (PEG) and polyaspartate, so-called PEG-polyaspartate described previously (Yokoyama et al. 1990; 1991a, b, c; Kataoka et al. 1993), were used. PTX was incorporated into polymeric micelles formed by physical entrapment utilizing hydrophobic interactions between PTX and the block copolymer polyaspartate chain. After screening of many candidate substances, 4-phenyl-1-butanol was employed for the chemical modification of the polyaspartate block to increase its hydrophobicity. Treating with a condensing agent, 1,3-diisopropylcarbodiimide, the half of carboxyl groups on the polyaspartate were esterified with 4-phenyl-1-butanol. Molecular weight of the polymers was determined to be approximately 20,000, (PEG block: 12,000; modified polyaspartate block: 8000). NK105 was prepared by facilitating the self-association of NK105 polymers and PTX. NK105 was obtained as a freeze-dried formulation and contained *ca.* 23% (w/w) of PTX, as determined by reversed-phase liquid-chromatography using an ODS column with mobile phase consisting of acetonitrile and water (9:11, v/v) and detection of ultraviolet absorbance at 227 nm. Finally, NK105, a PTX-incorporating polymeric micellar nanoparticle formulation with a single and narrow size distribution, was obtained. The weight-average diameter of the nanoparticles was approximately 85 nm ranging from 20 to 430 nm.

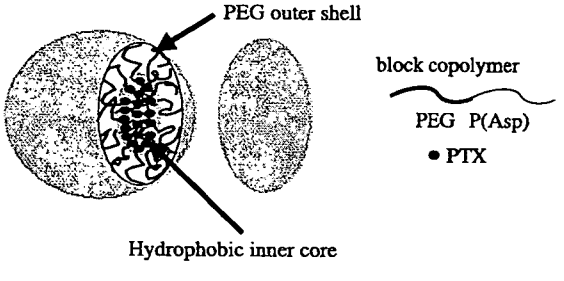

Figure 1. Preparation and characterization of NK105. The micellar structure of NK105 PTX was incorporated into the inner core of the micelle.

Pharmacokinetics and pharmacodynamics of NK105

Colon 26-bearing CDF1 mice were given a single iv injection of PTX 50 or 100 mg/kg, or of NK105 at an equivalent dose of PTX. Subsequently, the time-course changes in the plasma and tumour levels of PTX were determined in the PTX and NK105 administration groups; furthermore, the pharmacokinetic parameters of each group were also determined. NK105 exhibited slower clearance from the plasma than PTX, while NK105 was present in the plasma for up to 72 h after injection; PTX was not detected after 24 h or later of injection. The plasma concentration at 5 min ($C_{5\,min}$) and the AUC of NK105 were 11- to 20-fold and 50- to 86-fold higher for NK105 than for PTX, respectively. Furthermore, the half-life at the terminal phase ($t_{1/2}z$) was 4–6 times longer for NK105 than for PTX. The maximum concentration (C_{max}) and AUC of NK105 in Colon 26 tumours were approximately 3 times and 25 times higher for NK105 than for PTX, respectively. NK105 continued to accumulate in the tumours until 72 h after injection. The tumour PTX concentration was higher than 10 μg/g even at 72 h after the intravenous injection of NK105 50 and 100 mg/kg. By contraries, the tumour PTX concentrations at 72 h after the intravenous administration of free PTX 50 and 100 mg/kg were below detection limits and less than 0.1 μg/g, respectively.

In vivo *antitumour activity*

BALB/c mice bearing s.c. HT-29 colon cancer tumours showed decreased tumour growth rates after the administration of PTX and NK105. However, NK105 exhibited superior antitumour activity as compared with PTX ($P < 0.001$). The

antitumour activity of NK105 administered at a PTX-equivalent dose of 25 mg/kg was comparable to that obtained after the administration of free PTX 100 mg/kg. Tumour suppression by NK105 increased in a dose-dependent manner. Tumours disappeared after the first dosing to mice treated with NK105 at a PTX-equivalent dose of 100 mg/kg, and all mice remained tumour-free thereafter. In addition, less weight loss was induced in mice which were given NK105 100 mg/kg than in those which were given the same dose of free PTX.

Neurotoxicity of PTX and NK105

Treatment with PTX has resulted in cumulative sensory-dominant peripheral neurotoxicity in humans, characterized clinically by numbness and/or paraesthesia of the extremities. Pathologically, axonal swelling, vesicular degeneration, and demyelination were observed. We, therefore, examined the effects of free PTX and NK105 using both electrophysiological and morphological methods.

Prior to drug administration, there were no significant differences in the amplitude of caudal sensory nerve action potential (caudal SNAP) between two drug administration groups. On day 6 after the last dosing (at week 6), the amplitude of the caudal SNAP in the control group increased in association with rat maturation. The amplitude was significantly smaller in the PTX group than in the control group ($P < 0.01$), while the amplitude was significantly larger in the NK105 group than in the PTX group ($P < 0.05$) and was comparable between the NK105 group and the control group (Figure 2). Histopathological examination of longitudinal paraffin-embedded sections of the sciatic nerve 5 days after the sixth weekly injection revealed degenerative changes. The NK105 administration group showed only a few degenerative myelinated fibers in contrast to the PTX administration group which indicated markedly more numerous degenerative myelinated fibers.

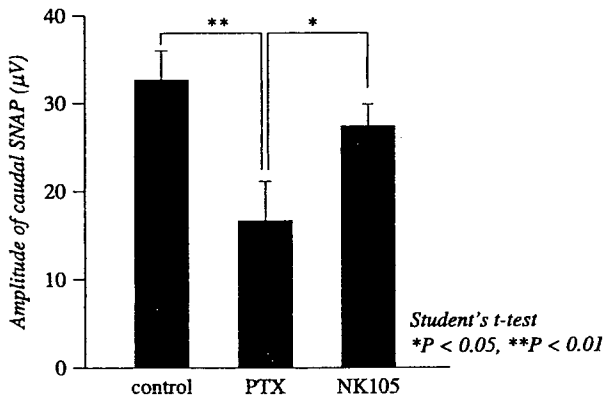

Figure 2. Effects of PTX or NK105 on the amplitude of rat caudal sensory nerve action potentials as examined 5 days after weekly injections for 6 weeks. Rats ($n = 14$) were injected with NK105 or PTX at a PTX-equivalent dose of 7.5 mg/kg. About 5% glucose was also injected in the same manner to animals in the control group.

Clinical study

A phase I study was designed to determine maximum tolerated dose (MTD), DLTs, the recommended dose (RD) for phase II and the pharmacokinetics of NK105 (Kato et al.).

NK105 was administered by 1-hour intravenous infusion every 3 weeks without anti-allergic premedication. The starting dose was 10 mg PTX equivalent/m^2, and dose escalated according to the accelerated titration method. To date, 17 patients (pts) have been treated at the following doses: 10 mg/m^2 ($n = 1$); 20 mg/m^2 ($n = 1$); 40 mg/m^2 ($n = 1$); 80 mg/m^2 ($n = 1$); 110 mg/m^2 ($n = 3$); 150 mg/m^2 ($n = 5$); 180 mg/m^2 ($n = 5$). Tumor types treated have included: pancreatic ($n = 9$), bile duct ($n = 5$), gastric ($n = 2$), and colon ($n = 1$). Neutropenia has been the predominant hematological toxicity and grade 3 or 4 neutropenia was observed in pts treated at 110, 150 and 180 mg/m^2. One patient at 180 mg/m^2 developed grade 3 fever. No other grade 3 or 4 non-hematological toxicity including neuropathies was observed. DLTs were observed in pts with at the 180 mg/m^2 (grade 4 neutropenia lasting for more than 5 days), which was determined as MTD. Allergic reactions were not observed in any of the patients except one patient at the 180 mg/m^2. A partial response was observed in one pancreatic cancer pt who received more than 12 courses of NK105 (Figure 3). Despite of the long time usage, only grade 1 or 2 neuropathy was observed by modifying the dose or period of drug administration. Colon and gastric cancer pts experienced stable disease lasting 10 and 7 courses, respectively. The C_{max} and AUC of NK105 showed dose-dependent characteristics. The plasma AUC of NK105 at 180 mg/m^2 was approximately 30-fold higher than that of commonly-used paclitaxel formulation.

Accrual is ongoing at the 150 mg/m^2 dose level to determine RD. DLT was grade 4 neutropenia. NK105 generates prolonged systemic exposure to PTX in plasma. Tri-weekly 1-hour infusion of NK105 was feasible and well tolerated, with antitumor activity in pancreatic cancer pt. NK105 is planning to be evaluated in Phase II studies of patients with pancreatic, gastric, or ovarian cancer.

NC-6004, cisplatin-incorporating micellar nanoparticle

Cisplatin [*cis*-dichlorodiammineplatinum (II): CDDP] is a key drug in the chemotherapy for cancers, including lung, gastrointestinal, and genitourinary cancer (Roth 1996; Horwich et al. 1997). However, we often find that it is necessary to

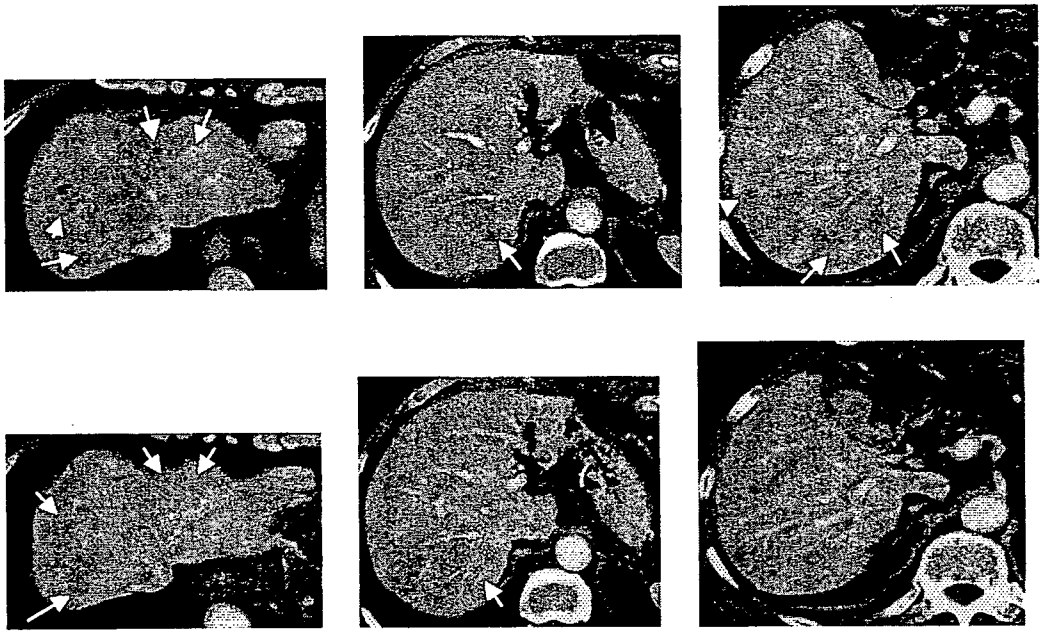

Figure 3. Serial CT scans. (A) A 60-year-old male with pancreatic cancer who was treated with NK105 at a dose level of 150 mg/m^2. Baseline scan (upper panels) showing multiple metastasis in the liver. Partial response, characterized by a more than 90% decrease in the size of the liver metastasis (lower panels) compared with the baseline scan. The antitumor response was maintained for nearly 1 year.

discontinue treatment with CDDP due to its adverse reactions, e.g. nephrotoxicity and neurotoxicity, despite its persisting effects (Pinzani et al. 1994). Platinum analogues, e.g. carboplatin and oxaliplatin (Cleare et al. 1978), have been developed to date to overcome these CDDP-related disadvantages. Consequently, these analogues are becoming the standard drugs for ovarian cancer (du Bois et al. 2003) and colon cancer (Cassidy et al. 2004). However, those regimens including CDDP are considered to constitute the standard treatment for lung cancer, stomach cancer, testicular cancer (Horwich et al. 1997), and urothelial cancer (Bellmunt et al. 1997). Therefore, the development of a DDS technology is anticipated, which would offer the better selective accumulation of CDDP into solid tumours while lessening its distribution into normal tissue.

Preparation and characterization of NC-6004

NC-6004 were prepared according to the slightly modified procedure reported by Nishiyama et al. (2003) (Figure 4). NC-6004 consists of PEG, a hydrophilic chain which constitutes the outer shell of the micelles, and the coordinate complex of poly(glutamic acid) (P(Glu)) and CDDP, a polymer-metal complex-forming chain which constitutes the inner core of the micelles. The molecular weight of PEG-P(Glu) as a sodium salt was approximately 18,000 (PEG: 12,000; P(Glu): 6000). The CDDP-incorporated polymeric micelles were clearly discriminated from typical micelles from amphiphilic block copolymers. The driving force of the formation of the CDDP-incorporated micelles is the ligand substitution of platinum(II) atom from chloride to carboxylate in the side chain of P(Glu). The molar ratio of CDDP to the carboxyl groups in the copolymers was 0.71 (Nishiyama et al. 2003). A narrowly distributed size of polymeric micelles (30 nm) was confirmed by the dynamic light scattering (DLS) measurement. Also, the static light scattering (SLS) measurement revealed that the CDDP-loaded micelles showed no dissociation upon dilution and the CMC was less than 5×10^{-7}, suggesting remarkable stability compared with typical micelles from amphiphilic block copolymers (Nishiyama et al. 2003). It is assumed that the interpolymer cross-linking by Pt(II) atom might contribute to stabilization of the micellar structure.

The release rates of CDDP from NC-6004 were 19.6 and 47.8% at 24 and 96 h, respectively. In distilled water, furthermore, NC-6004 was stable without releasing cisplatin.

Pharmacokinetics and pharmacodynamics

FAAS could measure serum concentrations of platinum up to 48 h after i.v. injection of NC-6004 but could measure them only up to 4 h after i.v. injection of CDDP. NC-6004 showed a very long blood retention profile as compared with CDDP. The AUC_{0-t} and C_{max} values were significantly higher in animals given NC-6004 than in animals given CDDP, namely, 65-fold and 8-fold, respectively, ($P < 0.001$ and 0.001, respectively). Furthermore, the CL_{tot} and Vss values were significantly lower in animals given NC-6004 than in animals given

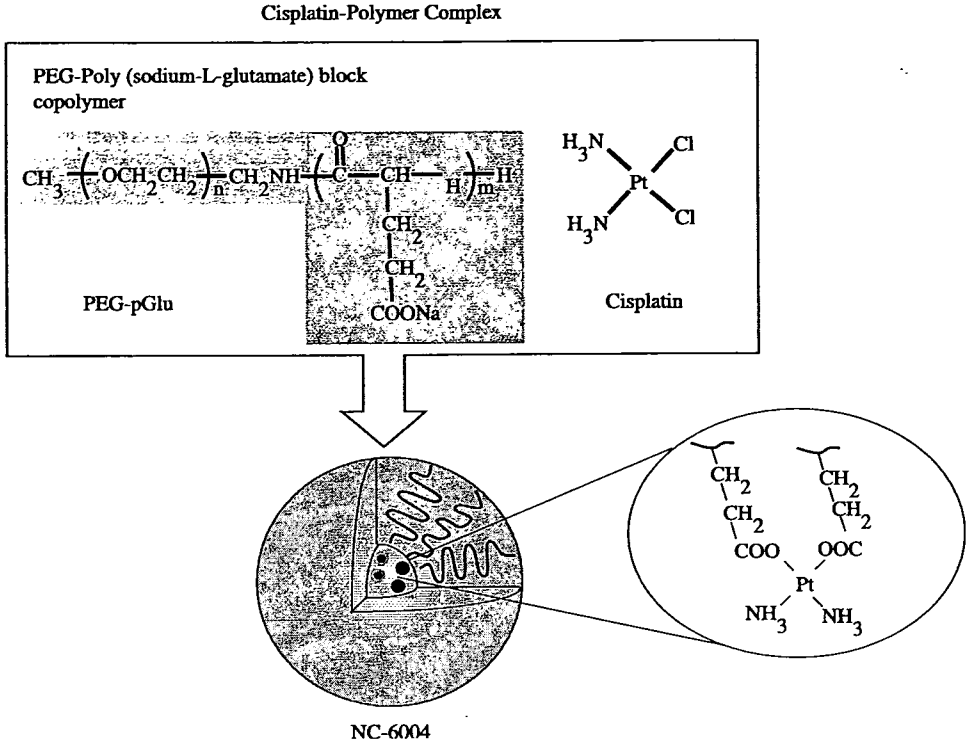

Figure 4. Preparation and characterization of cisplatin-incorporating polymeric micelles (NC-6004). Chemical structures of cisplatin (CDDP) and polyethylene glycol poly(glutamic acid) block copolymers [PEG-P(Glu) block copolymers], and the micellar structures of CDDP-incorporating polymeric micelles (NC-6004).

CDDP, i.e. one-nineteenth and one-seventy fifth, respectively, ($P < 0.01$ and 0.01, respectively).

Regarding the concentration–time profile of platinum in various tissues after i.v. injection of CDDP or NC-6004, all organs measured exhibited the highest concentrations of platinum within 1 h after administration in all animals given CDDP. Furthermore, animals given NC-6004 exhibited the highest tissue concentrations of platinum in the liver and spleen at late time points (24 and 48 h after administration, respectively). However, the concentrations decreased on day 7 after administration. In addition, and in a similar manner to other drugs, which are incorporated in polymeric carriers, NC-6004 demonstrated accumulation in organs of the reticuloendothelial system, e.g. liver and spleen. At 48 h after administration, tissue concentrations of platinum in the liver and spleen were 4.6- and 24.4-fold higher for NC-6004 than for CDDP. On the other hand, a marked increase in tissue platinum concentration was observed immediately after administration in the kidneys of animals given CDDP. Renal platinum concentration at 10 min and 1 h after administration were 11.6- and 3.1-fold lower, respectively, in animals given NC-6004 than in animals given CDDP. Furthermore, the maximum concentration (C_{max}) in the kidney was 3.8-fold lower at the time of NC-6004 administration than at the time of CDDP administration.

Regarding the tumour accumulation of platinum, tumour concentrations of platinum peaked at 10 min after administration of CDDP. On the other hand, tumour concentrations of platinum peaked at 48 h after administration of NC-6004. The maximum concentration (C_{max}) in tumour was 2.5-fold higher for NC-6004 than for CDDP ($P < 0.001$). Furthermore, the tumour AUC was 3.6-fold higher for NC-6004 than for CDDP (81.2 and 22.6 μg/ml h in animals given NC-6004 and CDDP, respectively).

In vivo *antitumour activity*

BALB/c nude mice implanted with a human gastric cancer cell line MKN-45 showed decreased tumour growth rates after i.v. injection of CDDP and NC-6004. In the administration of CDDP, the CDDP 5 mg/kg administration group showed a significant decrease ($P < 0.01$) in tumour growth rate as compared with the control group. However, the NC-6004 administration groups at the same dose levels as CDDP showed no significant difference in tumour growth rate. Regarding time-course changes in body weight change rate, the CDDP 5 mg/kg administration group showed a significant decrease ($P < 0.001$) in body weight as compared with the control group. On the other hand, NC-6004 administration group did not show a decrease in body weight as compared with the control group.

Nephrotoxicity of CDDP and NC-6004

In the CDDP 10 mg/kg administration group, 4 of 12 rats died from toxicity within 7 days after drug administration. No deaths occurred in the NC-6004 10 mg/kg administration group. Regarding renal function, the BUN concentrations on day 7 after the administration of 5% glucose, CDDP 10 mg/kg, and NC-6004 10 mg/kg were 20.8 ± 3.0, 65.3 ± 44.4 and 20 ± 4.5 mg/dl, respectively. The plasma concentrations of creatinine on day 7 after the administration of 5% glucose, CDDP 10 mg/kg, and NC-6004 10 mg/kg were 0.27 ± 0.03, 0.68 ± 0.23 and 0.28 ± 0.04 mg/dl, respectively. The CDDP 10 mg/kg administration group showed significantly higher plasma concentrations of BUN and creatinine as compared with the control group ($P < 0.05$ and 0.001, respectively), with the NC-6004 10 mg/kg administration group ($P < 0.05$ and 0.001, respectively) (Figure 5). Light microscopy indicated tubular dilation with flattening of the lining cells of the tubular epithelium in the kidney from all animals in the CDDP 10 mg/kg administration group. On the other hand, no histopathological change was observed in the kidneys from all animals in the NC-6004 10 mg/kg administration group.

Neurotoxicity of CDDP and NC-6004

Neurophysiological examination revealed that motor nerve conduction velocities (MNCVs) in animals given 5% glucose, CDDP, and NC-6004 were 44.2 ± 3.5, 40.94 ± 5.08 and 40.62 ± 0.63 m/s, respectively. No significant difference was found among the groups with respect to MNCV. Furthermore, sensory nerve conduction velocities (SNCVs) in animals given 5% glucose, CDDP, and NC-6004 were 42.86 ± 8.07, 35.48 ± 4.91 and 43.74 ± 5.3 m/s, respectively. Animals given NC-6004 showed no delay in SNCV as compared with animals given 5% glucose. On the other hand, animals given CDDP showed a significant delay ($P < 0.05$) in SNCV as compared with animals given NC-6004 (Figure 6). The analysis by ICP-MS on sciatic nerve concentrations of platinum could not detect platinum in the sciatic nerve from animals given 5% glucose (data not shown). Sciatic nerve concentrations of platinum

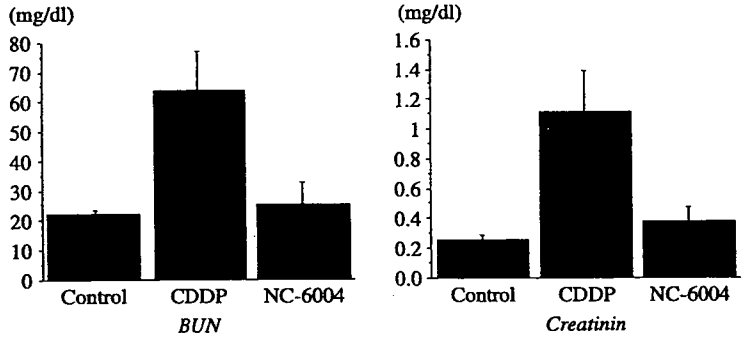

Figure 5. Nephrotoxicity of CDDP and NC-6004. Plasma concentrations of blood urea nitrogen (BUN) and creatinine were measured after a single i.v. injection of 5% glucose ($n = 8$), CDDP at a dose of 10 mg/kg ($n = 12$), NC-6004 at a dose of 10 mg/kg ($n = 13$) on a CDDP basis.

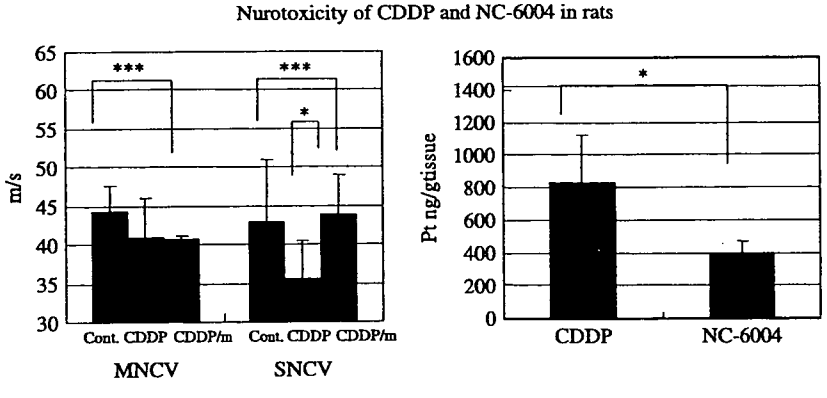

Figure 6. Neurotoxicity of CDDP and NC-6004 in rats. Rats ($n = 5$) were given CDDP (2 mg/kg), NC-6004 (an equivalent dose of 2 mg/kg CDDP), or 5% glucose, all intravenously twice a week, 11 administrations in total. Sensory nerve conduction velocity (SNCV) and motor nerve conduction velocity (MNCV) of the sciatic nerve at week 6 after the initial administration. The platinum concentration in the sciatic nerve. Rats were given CDDP (5 mg/kg, $n = 5$), NC-6004 (an equivalent dose of 5 mg/kg CDDP, $n = 5$), or 5% glucose ($n = 2$), all intravenously twice a week, four administrations in total. On day 3 after the final administration, a segment of the sciatic nerve was removed and the platinum concentration in the sciatic nerve was measured by ICP-MS. The data are expressed as the mean ± SD $*P < 0.05$.